arXiv:1812.01736v3 [physics.comp-ph] 3 Apr 2019

Machine Learning of coarse-grained Molecular Dynamics Force Fields

Jiang Wang,[†,‡] Simon Olsson,[¶] Christoph Wehmeyer,[¶] Adrià Pérez,[§] Nicholas E. Charron,[†,‖] Gianni de Fabritiis,[§,⊥] Frank Noé,[*,¶,†,‡] and Cecilia Clementi[*,†,‡,‖,¶]

†*Rice University, Center for Theoretical Biological Physics, Houston, Texas 77005, United States*

‡*Rice University, Department of Chemistry, Houston, Texas 77005, United States*

¶*Freie Universität Berlin, Department of Mathematics and Computer Science, Arnimallee 6, 14195 Berlin, Germany*

§*Computational Science Laboratory, Universitat Pompeu Fabra, PRBB, C/ Dr Aiguader 88, 08003, Barcelona, Spain*

‖*Rice University, Department of Physics, Houston, Texas 77005, United States*

⊥*Institucio Catalana de Recerca i Estudis Avanats (ICREA), Passeig Lluis Companys 23, Barcelona 08010, Spain*

E-mail: frank.noe@fu-berlin.de; cecilia@rice.edu

Abstract

Atomistic or ab-initio molecular dynamics simulations are widely used to predict thermodynamics and kinetics and relate them to molecular structure. A common approach to go beyond the time- and length-scales accessible with such computationally expensive simulations is the definition of coarse-grained molecular models. Existing coarse-graining approaches define an effective interaction potential to match defined properties of high-resolution models or experimental data. In this paper, we reformulate coarse-graining as a supervised machine learning problem. We use statistical learning theory to decompose the coarse-graining error and cross-validation to select and compare the performance of different models. We introduce CGnets, a deep learning approach, that learns coarse-grained free energy functions and can be trained by a force matching scheme. CGnets maintain all physically relevant invariances and allow one to incorporate prior physics knowledge to avoid sampling of unphysical structures. We show that CGnets can capture all-atom explicit-solvent free energy surfaces with models using only a few coarse-grained beads and no solvent, while classical coarse-graining methods fail to capture crucial features of the free energy surface. Thus, CGnets are able to capture multi-body terms that emerge from the dimensionality reduction.

Introduction

Recent technological and methodological advances have made possible to simulate macromolecular systems on biologically relevant timescales[1–3]. For instance, one can simulate binding, folding and conformation changes of small to intermediate-size proteins on timescales of milliseconds, seconds or beyond[4–8]. However, the extensive sampling of large macromolecular complexes on biological timescales at atomistic resolution is still out of reach. For this reason, the design of simplified, yet predictive models is of great interest[9–11], in particular, to interpret the experimental data that are becoming increasingly accessible in

high throughput and resolution. Experimental data provide a partial view of certain aspects of a macromolecular system but do not directly give a full dynamical representation and simulation can help obtain a more comprehensive understanding[12–14]. As it is clear that not every single atom is important in determining the relevant collective features of biomolecular dynamics and function, simplified models could provide more insights into the general physicochemical principles regulating biophysical systems at the molecular level. Here we use recent advances in machine learning to design optimal reduced models to reproduce the equilibrium thermodynamics of a macromolecule.

Significant effort has been devoted in the last few years to apply machine learning (e.g., deep neural network or kernel methods) to learn effective models from detailed simulations[15–19], and specifically to learn potential energy surfaces from quantum mechanical calculations on small molecules[20–36]. In principle a similar philosophy could be used to define models at lower resolutions, that is to learn the effective potential energy of coarse-grained (CG) models from fine-grained (e.g., atomistic) molecular dynamics (MD) simulation data[37–41].

There are however important differences. In the definition of potential energy surfaces from quantum calculations, the relevant quantity to reproduce is the energy, and it is relatively straightforward to design a loss function for a neural network to minimize the difference between the quantum mechanical and classical energy (and forces[25,33]) over a sample of configurations. In contrast, in the definition of a CG model, the potential energy can not be matched because of the reduction in dimension, and it is important to define what are the properties of the system that need to be preserved by the coarse-graining. The approximation of free-energy surfaces, e.g. from enhanced sampling simulations, is therefore a related problem[42–44].

Several approaches have been proposed to design effective CG energy functions for large molecular systems that either reproduce structural features of atomistic models (bottom-up)[45–50] or reproduce macroscopic properties for one or a range of systems (top-down)[12–14,51–54]. Popular bottom-up approaches choose that the CG model reproduce the canonical configuration distribution determined by the atomistic model. For instance, one may want to be able to represent the different metastable states populated by a protein undergoing large conformational changes. One of the difficulties in the practical application of these methods has been that, in general, a CG potential optimally reproducing selected properties of a macromolecular system includes many-body terms that are not easily modeled in the energy functions.

Here, we formulate the well-known force matching procedure for coarse-graining as a supervised machine learning problem. Previously, coarse-graining has been mostly discussed as a fitting procedure, but the aim of machine learning is to find a model that has minimal prediction error on data not used for the training. We use classical statistical learning theory to show that the force matching error can be decomposed into Bias, Variance and Noise terms and explain their physical meaning. We also show that the different CG models can be ranked using their cross-validation score.

Second, we discuss a class of neural networks, which we refer to as CGnets, for coarse-graining molecular force systems. CGnets have a lot of similarities with neural networks used to learn potential energy surfaces from quantum data, such as enforcing the relevant invariances (e.g., rotational and translational invariance of the predicted energy, equivariance of the predicted force). In contrast to potential energy networks, CGnets predict a free energy (potential of mean force) and then use the gradient of this free energy with respect to the input coordinates to compute a mean force on the CG coordinates. As the CG free energy is not known initially, only the force information can be used to train the network.

Third, CGnets are extended to regularized CGnets. Using a generic function approximator such as a neural network to fit the CG force field from training data only may lead to force predictions that are "catastrophically wrong" for configurations not captured by the training

data, i.e., predictions of forces in the direction of increasingly unphysical states that lead to diverging and unrealistic simulation results. We address this problem by adding a prior energy to the free energy network that does not compromise the model accuracy within the training data region, but ensures that the free energy approaches infinity for unphysical states, resulting in a restoring force towards physically meaningful states.

Finally, we demonstrate that CGnets succeed in learning the CG mean force and the CG free energy for a 2D toy model, as well as for the coarse-graining of all-atom explicit-solvent simulations of (i) alanine dipeptide to a CG model with 5 particles and no solvent, and (ii) the folding/unfolding of the polypeptide Chignolin to a CG model consisting only of the protein C_α atoms and no solvent. We show explicitly that CGnets achieve a systematically better performance than classical CG approaches which construct the CG free energy as a sum of few-body terms. In the case of the Chignolin protein, the classical few-body model can not reproduce the folding/unfolding dynamics. On the contrary, the inherently multi-body CGnet energy function approximates the all-atom folding/unfolding landscape well and captures all free energy minima. This study highlights the importance of machine learning and generic function approximators in the CG problem.

Theory and methods

Here we introduce the main theoretical concepts and define the machine learning problems involved in coarse-graining using the force matching principle, and introduce CGnets and regularized CGnets. The more practically inclined reader may skip to the Section "CGnets: Learning CG force fields with neural networks".

Coarse-graining with thermodynamic consistency

We first define what we mean by coarse-graining and which physical properties shall be preserved in the coarse-grained model.

The starting point in the design of a molecular model with resolution coarser than atomistic is the definition of the variables. The choice of the coarse coordinates is usually made by replacing a group of atoms by one effective particle. Because of the modularity of a protein backbone or a DNA molecule, popular models coarse-grain a macromolecule to a few interaction sites per residue or nucleotide, e.g., the C_α and C_β atoms for a protein[51,54–56]. Alternative schemes have also been proposed for the partitioning of the atoms into coarse-grained coordinates[57,58]. In general, given a high-dimensional atomistic representation of the system $\mathbf{r} \in \mathbb{R}^{3N}$, a CG representation is given by a coordinate transformation to a lower-dimensional space:

$$\mathbf{x} = \xi(\mathbf{r}) \in \mathbb{R}^{3n} \tag{1}$$

with $n < N$. Here we assume that ξ is linear, i.e. there is some coarse-graining matrix $\Xi \in \mathbb{R}^{3n\times 3N}$ that clusters atoms to coarse-grained beads: $\mathbf{x} = \Xi\mathbf{r}$.

The aim is to learn a coarse-grained energy function $U(\mathbf{x};\boldsymbol{\theta})$ that will be used in conjunction with a dynamical model, e.g., Langevin dynamics, to simulate the CG molecule. $\boldsymbol{\theta}$ are the parameters of the coarse-grained model – in classical CG approaches these are parameters of the potential energy function, such as force constants and partial charges, while here they denote the weights of the neural network.

A common objective in coarse-graining methods is to preserve the equilibrium distribution, i.e. the equilibrium distribution of the coarse-grained model shall be as close as possible to the equilibrium distribution of the atomistic model when mapped to the CG coordinates. We will be using a simulation algorithm for the dynamics such that the system's equilibrium distribution is identical to the Boltzmann distribution of the employed potential U; therefore this objective can be achieved by enforcing the thermodynamic consistency:

$$U(\mathbf{x};\boldsymbol{\theta}) \equiv -k_B T \ln p^{CG}(\mathbf{x}) + \text{const}, \tag{2}$$

where $k_B T$ is the thermal energy with Boltzmann constant k_B and temperature T, and

the probability distribution $p^{CG}(\mathbf{x})$ is the equilibrium distribution of the atomistic model, mapped to the CG coordinates:

$$p^{CG}(\mathbf{x}) = \frac{\int \mu(\mathbf{r})\delta\left(\mathbf{x} - \xi(\mathbf{r})\right) d\mathbf{r}}{\int \mu(\mathbf{r}) d\mathbf{r}} \tag{3}$$

and $\mu(\mathbf{r}) = \exp\left(-V(\mathbf{r})/k_B T\right)$ is the Boltzmann weight associated with the atomistic energy model $V(\mathbf{r})$. Note that the additive constant in (2) can be chosen arbitrarily. Therefore this constant will be omitted in the expressions below, which means that it will absorb normalization constants that are not affecting the CG procedure, such as the logarithm of the partition function.

Several methods have been proposed for defining a coarse-grained potential $U(\mathbf{x})$ that variationally approximates the consistency relation (3) at a particular thermodynamic state (temperature, pressure etc.) Two popular approaches are the multi-scale coarse-graining (force-matching)[48,59] and the relative entropy method[50] (the two approaches are connected[60]).

CG parameter estimation as a machine learning problem

Here, we follow the force-matching scheme. It has been shown that thermodynamic consistency (2) is achieved when the CG model predicts the instantaneous CG forces with minimal mean square error[48,59]. We call the instantaneous atomistic forces $\mathbf{F}(\mathbf{r})$, and the instantaneous force projected on the CG coordinates $\xi(\mathbf{F}(\mathbf{r}))$. At the same time, the CG model predicts a force $-\nabla U(\mathbf{x};\boldsymbol{\theta})$ for a CG configuration $\mathbf{x}$. The force matching error is defined as:

$$\chi^2(\boldsymbol{\theta}) = \left\langle \left\| \xi(\mathbf{F}(\mathbf{r})) + \nabla U(\xi(\mathbf{r});\boldsymbol{\theta}) \right\|^2 \right\rangle_{\mathbf{r}}. \tag{4}$$

The average $\langle\cdot\rangle_{\mathbf{r}}$ is over the equilibrium distribution of the atomistic model, i.e., $\mathbf{r} \sim \mu(\mathbf{r})$.

We reiterate a result shown in[59] that has important consequences for using (4) in machine learning. For this, we introduce the mean force:

$$\mathbf{f}(\mathbf{x}) = \langle \xi(\mathbf{F}(\mathbf{r})) \rangle_{\mathbf{r}|\mathbf{x}} \tag{5}$$

where $\mathbf{r} \mid \mathbf{x}$ indicates the equilibrium distribution of $\mathbf{r}$ constrained to the CG coordinates $\mathbf{x}$, i.e. the ensemble of all atomistic configurations that map to the same CG configuration. Then we can decompose expression (4) as follows (see SI for derivation):

$$\chi^2(\boldsymbol{\theta}) = \text{PMF error}(\boldsymbol{\theta}) + \text{Noise} \tag{6}$$

with the terms

$$\begin{aligned} \text{PMF error}(\boldsymbol{\theta}) &= \langle \| \mathbf{f}(\xi(\mathbf{r})) + \nabla U(\xi(\mathbf{r});\boldsymbol{\theta}) \|^2 \rangle_{\mathbf{r}} \\ \text{Noise} &= \langle \| \xi(\mathbf{F}(\mathbf{r})) - \mathbf{f}(\xi(\mathbf{r})) \|^2 \rangle_{\mathbf{r}}. \end{aligned} \tag{7}$$

This loss function differs from the force matching loss function used in the learning of force fields from quantum data by the Noise term. The Noise term is purely a function of the CG map ξ (and when training with finite simulation data also of the dataset), and it cannot be changed by varying the parameters $\boldsymbol{\theta}$. As a result, the total force matching error cannot be made zero but it is bounded from below by $\chi^2(\boldsymbol{\theta}) \geq \text{Noise}$[59]. On the contrary, when matching force fields from quantum data, the error χ^2 approaches zero for a sufficiently powerful model. Physically, the Noise term arises from the fact that instantaneous forces on the CG coordinates vary in the different atomistic configurations associated with the same CG configuration. Here, we call this term Noise as it corresponds to the noise term known in statistical estimator theory for regression problems[61].

The learning problem is now to find a CG model and its parameters $\boldsymbol{\theta}$ that minimizes the PMF error term. In order to obtain a physical interpretation, we apply (1) and write the average purely in CG coordinates:

$$\begin{aligned} \text{PMF error}(\boldsymbol{\theta}) &= \langle \| \mathbf{f}(\mathbf{x}) + \nabla U(\mathbf{x};\boldsymbol{\theta}) \|^2 \rangle_{\mathbf{x}} \\ &= \langle \| \mathbf{f}(\mathbf{x}) - \hat{\mathbf{f}}(\mathbf{x};\boldsymbol{\theta}) \|^2 \rangle_{\mathbf{x}} \end{aligned}$$

This error term is the matching error between the mean force at the CG coordinates, $\mathbf{f}(\mathbf{x})$ and the CG forces predicted by the CG potential,

$$\hat{\mathbf{f}}(\mathbf{x};\boldsymbol{\theta}) = -\nabla U(\mathbf{x};\boldsymbol{\theta}). \tag{8}$$

Hence, the machine learning task is to find the

free energy U whose negative derivatives best approximate the mean forces in Eq (5), and U is thus called a potential of mean force (PMF). Eq. (8) implies that the mean force field $\hat{\mathbf{f}}$ is conservative, as it is generated by the free energy $U(\mathbf{x})$.

Machine learning the CG model is complicated by two aspects: (i) As the PMF error cannot be computed directly, its minimization in practice is accomplished by minimizing the variational bound (6). Thus, to learn $\mathbf{f}(\mathbf{x})$ accurately, we need to collect enough data "close" to every CG configuration $\mathbf{x}$ such that the learning problem is dominated by the variations in the PMFerror term and not by the variations in the Noise term. As a result, machine learning CG models typically requires more data points than force matching for potential energy surfaces; (ii) The free energy $U(\mathbf{x})$ is not known a priori, but must be learned. In contrast to fitting potential energy surfaces we can therefore not directly use energies as inputs.

For a finite dataset $\mathbf{R} = (\mathbf{r}_1, ..., \mathbf{r}_M)$ with M samples, we define the force matching loss function by the direct estimator:

$$L(\boldsymbol{\theta}; \mathbf{R}) = \frac{1}{3Mn} \sum_{i=1}^{M} \left\| \xi(\mathbf{F}(\mathbf{r}_i)) + \nabla U(\xi(\mathbf{r}_i); \boldsymbol{\theta}) \right\|^2 \tag{9}$$

$$= \frac{1}{3Mn} \left\| \xi(\mathbf{F}(\mathbf{R})) + \nabla U(\xi(\mathbf{R}); \boldsymbol{\theta}) \right\|_F^2 . \tag{10}$$

Where $\xi(\mathbf{R}) = [\xi(\mathbf{r}_1), ..., \xi(\mathbf{r}_M)]^\top \in \mathbb{R}^{M \times 3n}$ and $\xi(\mathbf{F}(\mathbf{R})) = [\xi(\mathbf{F}(\mathbf{r}_1)), ..., \xi(\mathbf{F}(\mathbf{r}_M))]^\top \in \mathbb{R}^{M \times 3n}$ are data matrices of coarse-grained coordinates and coarse-grained instantaneous forces that serve as an input to the learning method, and F denotes the Frobenius norm.

CG hyper-parameter estimation as a machine learning problem

While Eq. (9) defines the training method, machine learning is not simply about fitting parameters for a given dataset, but rather about minimizing the expected prediction error (also called "risk") for data not used for training. This concept is important in order to be able to select an optimal model, i.e. in order to choose the hyper-parameters of the model, such as the type and number of neurons and layers in a neural network, or even to distinguish between different learning models such as a neural network and a spline model.

Statistical estimator theory is the field that studies optimal prediction errors[61]. To compute the prediction error, we perform the following thought experiment: We consider a fixed set of CG configurations $\mathbf{X} = [\mathbf{x}_1, ..., \mathbf{x}_M]^\top$ at which we want to fit the mean forces. We assume that these configurations have been generated by MD or MCMC such that the full atomistic configurations, $\mathbf{R} = (\mathbf{r}_1, ..., \mathbf{r}_M)$, are Boltzmann distributions conditioned on the CG configurations, i.e. $\mathbf{r}_i \sim \mathbf{r} \mid \mathbf{x}_i$. Now we ask: if we repeat this experiment, i.e. in every iteration we produce a new set of all-atom configurations $\mathbf{r}_i \sim \mathbf{r} \mid \mathbf{x}_i$, and thereby a new set of instantaneous forces on the CG configurations, what is the expected prediction error, or risk of the force matching error, $\mathbb{E}\left[L(\boldsymbol{\theta}; \mathbf{R})\right]$? More formally:

1. Given CG coordinates $\mathbf{X}$, generate training set $\mathbf{R}^{\text{train}} \sim \mathbf{R} \mid \mathbf{X}$ and find $\hat{\boldsymbol{\theta}} = \arg\min_{\boldsymbol{\theta}} L(\boldsymbol{\theta}; \mathbf{R}^{\text{train}})$.
2. Generate test set $\mathbf{R}^{\text{test}} \sim \mathbf{R} \mid \mathbf{X}$ and compute $L(\hat{\boldsymbol{\theta}}; \mathbf{R}^{\text{test}})$

where $\mathbf{R}^{\text{train}}$ and $\mathbf{R}^{\text{test}}$ are two independent realizations. Although we cannot execute this thought experiment in practice, we can approximate it by cross-validation, and we can obtain insightful expressions for the form of the expected prediction error. As the loss function in force matching is a least squares regression problem, the form of the expected prediction error is well known (see SI for a short derivation), and can be written as:

$$\mathbb{E}\left[L(\boldsymbol{\theta}; \mathbf{R})\right] = \text{Bias}^2 + \text{Var} + \text{Noise} \tag{11}$$

with the Noise term as given in Eq. (7) and the

bias and variance terms given by:

$$\text{Bias}^2 = \left\|\mathbf{f}(\mathbf{X}) - \bar{\mathbf{f}}(\mathbf{X})\right\|_F^2 \tag{12}$$

$$\text{Var} = \mathbb{E}\left[\left\|\bar{\mathbf{f}}(\mathbf{X}) + \nabla U(\mathbf{X})\right\|_F^2\right] \tag{13}$$

where

$$\bar{\mathbf{f}}(\mathbf{X}) = \mathbb{E}\left[-\nabla U(\mathbf{X})\right]$$

is the mean estimator, i.e. the average force field learnt when the training is repeated many times for different data realizations. The terms in (12-13) have the following meaning: Eq. (12) is the expected error between the mean forces and the average predicted force field, it is therefore the systematic bias of the machine learning model. The variance (13) is the fluctuation of the individual estimates from single training procedures around the mean estimator and thus represents the estimator's fluctuation due to finite-sample effects.

As the optimal model minimizes the PMF error, it must balance bias and variance. These contributions are typically counteracting: A too simple model (e.g., too small neural network) typically leads to low variance but high bias, and it corresponds to "underfitting" the data. A too complex model (e.g., too large neural network) leads to low bias but large variance, and it corresponds to "overfitting" the data. The behavior of bias, variance and estimator error for a fixed data set size is illustrated in Fig. 1.

The optimum at which bias and variance balance depends on the amount of data used, and in the limit of an infinitely large dataset, the variance is zero and the optimal model can be made very complex so as to also make the bias zero. For small datasets, it is often favorable to reduce the model complexity and accept significant bias, in order to avoid large variance.

In order to implement model selection, we approximate the "ideal" iteration above by the commonly used cross-validation method[62,63] and then choose the model or hyper-parameter set that has the minimal cross-validation score. In cross-validation, the estimator error (11) is estimated as the validation error, averaged over different segmentations of all available data into training and validation data.

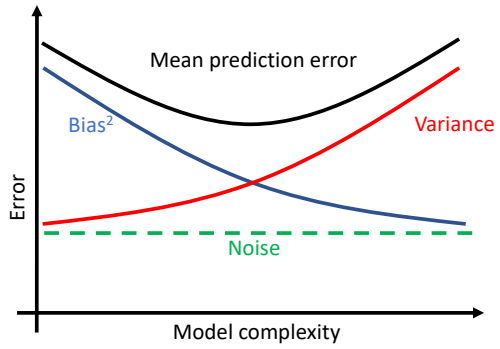


Figure 1: Typical bias-variance tradeoff for fixed data set size, indicating the balance between underfitting and overfitting. The noise level is defined by the CG scheme (i.e., which particles are kept and which are discarded) and is the lower bound for the mean prediction error.

CGnets: Learning CG force fields with neural networks

It is well known that the CG potential $U(\mathbf{x};\boldsymbol{\theta})$ defined by thermodynamic consistency may be a complex multi-body potential even if the underlying atomistic potential has only few-body interactions[59]. To address this problem, we use artificial neural networks (ANNs) to represent $U(\mathbf{x};\boldsymbol{\theta})$ as ANNs can approximate any smooth function on a bounded set of inputs, including multi-body functions[64].

Therefore, we use ANNs to model $U(\mathbf{x})$, train them by minimizing the loss (9) and select optimal models by minimizing the cross-validation loss. For the purpose of training CG molecular models, we would like to have the following physical constraints and invariances, which determine parts of the architecture of the neural network:

- **Differentiable free energy function**: In order to train $U(\mathbf{x};\boldsymbol{\theta})$ and simulate the associated dynamics by means of Langevin simulations, it must be continuously differentiable. As the present networks do not need to be very deep, vanishing gradients are not an issue and we select tanh activation functions here. After D nonlinear layers we always add one linear layer to map to one output neuron representing the free energy.
- **Invariances of the free energy**: The energy of molecules that are not subject

to an external field only depends on internal interactions and is invariant with respect to translation or rotation of the entire molecule. The CG free energy may also be invariant with respect to permutation of certain groups of CG particles, e.g. exchange of identical molecules, or certain symmetric groups within molecules. Compared to quantum-mechanical potential energies, permutation invariance is less abundant in CG. For example, permutation invariance does not apply to the α-carbons in a protein backbone (not even for identical amino acids), as they are ordered by the MD bonding topology. CGnets include a transformation:

$$\mathbf{y} = g(\mathbf{x})$$

from CG Cartesian coordinates $\mathbf{x}$ to a set of features that contain all desired invariances, and use the features $\mathbf{y}$ as an input to the network that computes the free energy, $U(g(\mathbf{x}); \boldsymbol{\theta})$. This transformation can be chosen in many different ways, e.g. by using local coordinate systems[34], two- or three-body correlation functions[20], permutation-invariant distance metrics[65–67], or by a learned representation[29]. In this work, only translation and rotation invariances are needed, and we hence choose the following features: distances between all pairs of CG atoms, the angles between three consecutive CG atoms, and the *cos* and *sin* of torsion angles defined by the CG atoms.

- **Conservative PMF**: The PMF is a conservative force field generated by the free energy (8). As in quantum potential energy learning[25,29], we enforce this requirement by computing the free energy U with a neural network and then adding a gradient layer to compute the derivatives with respect to the input coordinates:

$$\hat{\mathbf{f}}(\mathbf{x}; \boldsymbol{\theta}) = -\nabla_{\mathbf{x}} U(g(\mathbf{x}); \boldsymbol{\theta}).$$

Fig. 2a shows the neural network architecture resulting from these choices. The free energy network is D layers deep and each layer is W neurons wide. Additionally, we use L2 Lipschitz regularization[68] in the network, with a tunable parameter λ that regulates the strength of the regularization. Thus, (D, W, λ) are the remaining hyper-parameters to be selected (as discussed in the Results section).

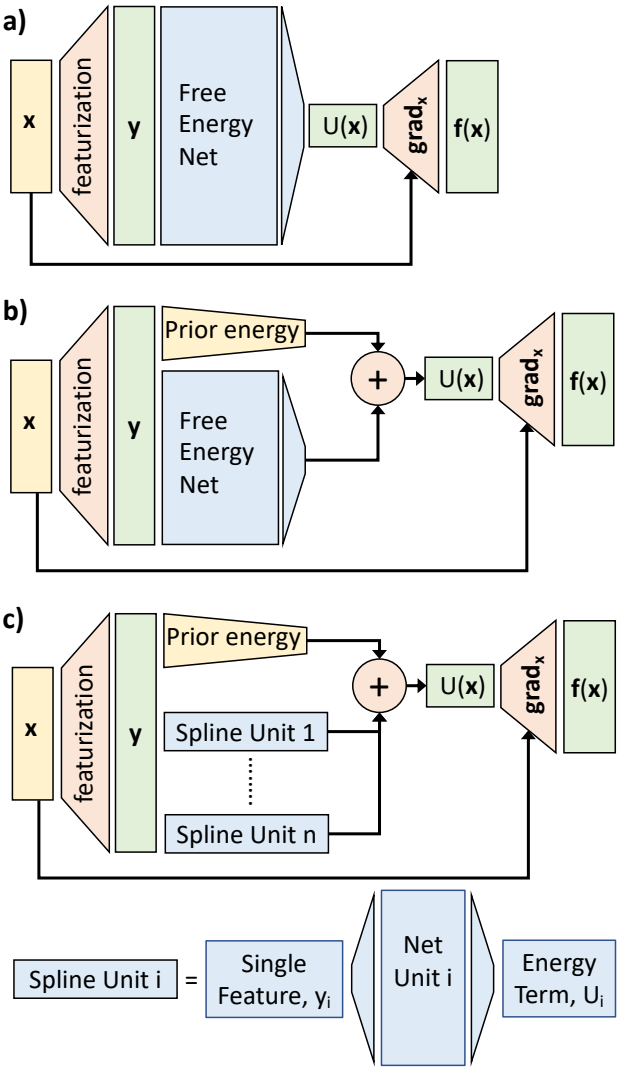


Figure 2: Neural network schemes. a) CGnet. b) Regularized CGnet with prior energy. c) Spline model representing a standard CG approach, for comparison. Each energy term is a function of only one feature, and the features are defined as all the bonds, angles, dihedrals, and non-bonded pairs of atoms.

Simulating the CGnet model

Once the neural network has been trained to produce a free energy $U(\mathbf{x})$, it can be used to simulate dynamical trajectories of the CG

model. Here we use over-damped Langevin dynamics to advance the coordinates of the CG model from $\mathbf{x}_t$ at time t to $\mathbf{x}_{t+\tau}$ after a time-step τ :

$$\mathbf{x}_{t+\tau} = \mathbf{x}_t - \tau \frac{D}{k_B T} \nabla U(\mathbf{x}_t) + \sqrt{2\tau D}\boldsymbol{\xi} \qquad (14)$$

where $\mathbf{x}_t$ is the CG configuration at time t (e.g., the x coordinate in the toy model, a 15-dimensional vector in the alanine dipeptide, and a 30-dimensional vector in the Chignolin applications presented below). $\boldsymbol{\xi}$ is Gaussian random noise with zero mean and identity as covariance matrix, τ is the integration time step, D is the diffusion constant of the system. In the following, we use reduced energy units, i.e. all energies are in multiples of $k_B T$.

Since the implementation of CGnet is vectorized, it is more efficient to compute free energies and mean forces for an entire batch of configurations, rather than a single configuration at a time. Therefore, we run simulations in parallel for the examples shown below. This is done by sampling 100 starting points randomly from atomistic simulations, coarse-graining them and then integrating (14) stepwise.

Regularizing the free energy with a baseline energy model

Training the free energy with a network as shown in Fig. 2a and subsequently using it in order to simulate the dynamics with Eq. (14) produces trajectories of new CG coordinates $\mathbf{x}_t$. When parts of the coordinate space are reached that are very different from any point in the training set, it is possible that the network makes unphysical predictions.

In particular, the atomistic force-field used to produce the training data has terms that ensure the energy will go towards infinity when departing from physical states, e.g. when stretching bonds or when moving atoms too close to each other. These regions will not be sampled in the underlying MD simulations, and therefore result in "empty" parts of configuration space that contain no training data. Simulating a network trained only on physically valid training data via Eq. (14) may still produce points $\mathbf{x}_t$ that enter this "forbidden regime" where bonds are overstretched or atoms start to overlap. At this point the simulation can become unstable if there is no regularizing effect ensuring that the predicted free energy $U(\mathbf{x};\boldsymbol{\theta})$ will increase towards infinity when going deeper into the forbidden regime.

Methods to modify a learning problem so as to reduce prediction errors are collectively known as "regularization" methods.[69] In order to avoid the catastrophically wrong prediction problem described above, we introduce regularized CGnets (Fig. 2b). In a regularized CGnet, we define the energy function as

$$U(\mathbf{x};\boldsymbol{\theta}) = U_0(\mathbf{x}) + U_{\mathrm{net}}(\mathbf{x};\boldsymbol{\theta}) \qquad (15)$$

where $U_{\mathrm{net}}(\mathbf{x};\boldsymbol{\theta})$ is a neural network free energy as before and $U_0(\mathbf{x})$ is a baseline energy that contains constraint terms that ensure basic physical behavior. Such baseline energies to regularize a more complex multi-body energy function have also been used in the machine learning of QM potential energy functions[70–72]. Note that (15) can still be used to represent any smooth free energy because $U_{\mathrm{net}}(\mathbf{x};\boldsymbol{\theta})$ is a universal approximator. The role of $U_0(\mathbf{x})$ is to enforce $U \to \infty$ for unphysical states $\mathbf{x}$ that are outside the training data.

As for many other regularizers, the baseline energy $U_0(\mathbf{x})$ in Eq. (15) takes the role of a prior distribution in a probabilistic interpretation: The equilibrium distribution generated by (15) becomes:

$$p^{CG}(\mathbf{x}) \propto \underbrace{\exp\left(-\beta U_0(\mathbf{x})\right)}_{\text{prior}} \exp\left(-\beta U_{net}(\mathbf{x};\theta)\right).$$

Here, $U_0(\mathbf{x})$ is simply a sum of harmonic and excluded volume terms. For the 2d toy model, a harmonic term in the form $U_0(x) = \frac{1}{2}k(x - x_0)^2$ is used, and the parameters k and x_0 are determined by the force matching scheme restricted to the scarcely populated regions defined by the 100 sampled points with highest and the 100 with lowest x-value (see Fig. 3).

For alanine dipeptide, we use harmonic terms for the distance between atoms that are adjacent (connected by covalent bonds) and for angles between three consecutive atoms. For each bond i, we use $U_{0,i}^{bond}(r_i; r_{i0}, k_{b,i}) = \frac{1}{2}k_{b,i}(r_i - r_{i0})^2$, where r_i is the instantaneous distance between the two consecutive atoms defining the bond, r_{i0} is the equilibrium bond length, and $k_{b,i}$ is a constant. Analogously, for each angle j, we use $U_{0,j}^{angle}(\theta_j; \theta_{j0}, k_{a,j}) = \frac{1}{2}k_{a,j}(\theta_j - \theta_{j0})^2$, where θ_j is the instantaneous value of the angle, θ_{j0} is the equilibrium value for the angle, and $k_{a,j}$ is a constant. When statistically independent, each such term would give rise to a Gaussian equilibrium distribution:

$$p(r_i) \propto \exp\left(-\frac{k_{b,i}(r_i - r_{i0})^2}{2k_BT}\right)$$
$$p(\theta_j) \propto \exp\left(-\frac{k_{a,j}(\theta_j - \theta_{j0})^2}{2k_BT}\right)$$

with mean $\mu = r_{i0}$ (or $\mu = \theta_{j0}$), and variance $\sigma^2 = k_BT/k_{b,i}$ (or $\sigma^2 = k_BT/k_{a,j}$). The prior energy is obtained by assuming independence between these energy terms and estimating these means and variances from the atomistic simulations.

For the application of CGnet to the protein Chignolin, an additional term is added to the baseline energy to enforce excluded volume and penalize clashes between non-bonded CG particles. In particular, we add a term $U_{rep}(r)$ for each pairwise distances between CG particles that are more distant than two covalent bonds, in the form:

$$U_{rep}(r) = \left(\frac{\sigma}{r}\right)^c \tag{16}$$

where the exponent c and effective excluded volume radius σ are two additional hyper-parameters that are optimized by cross-validation.

We note that in general one could use classical CG approaches with predefined energy functions to first define the prior CG energy U_0 , then use an ANN to correct it with multi-body terms.

Results

2-dimensional toy model

As a simple illustration, we first present the results on the coarse-graining of a two-dimensional toy model. The potential energy is shown in Fig. 3 and given by the expression:

$$\frac{V(x,y)}{k_BT} = \frac{1}{50}(x-4)(x-2)(x+2)(x+3) + \\ + \frac{1}{20}y^2 + \frac{1}{25}\sin\left(3(x+5)(y-6)\right). \tag{17}$$

The potential corresponds to a double well along the x-axis and a harmonic confinement along the y-axis. The last term in Eq. (17) adds small-scale fluctuations, appearing as small ripples in Fig. 3a.

The coarse-graining mapping is given by the projection of the 2-dimensional model onto the x-axis. In this simple toy-model, the coarse-grained free energy (potential of mean force) can be computed exactly (Fig. 3b):

$$\frac{U(x)}{k_BT} = -\ln\left[\int_{-\infty}^{+\infty}\exp\left(-\frac{V(x,y)}{k_BT}\right)dy\right].$$

We generate a long (one million time steps) simulation trajectory of the 2-dimensional model and use the x component of the forces computed along the trajectories in the loss function (9). We report below the resulting CG potential obtained by 1) using a feature regression, i.e. least square regression with a set of feature functions defined in SI Section B, and 2) a CGnet (regularized and unregularized).

Cross-validation is used to select the best hyper-parameters for the least square regression and the CGnet architectures. For the feature regression, the same cross-validation procedure as introduced in[1] was used, and returned a linear combination of four basis functions among the selected set (see Fig. S1a and SI for details). For the regularized CGnet, a two stage cross-validation is conducted, first choosing the depth D with a fixed width of $W = 50$, and then choosing the width W (Figs. S1b and S1c). The minimal prediction error is obtained with $D = 1$ (one hidden layer) and $W = 50$. For

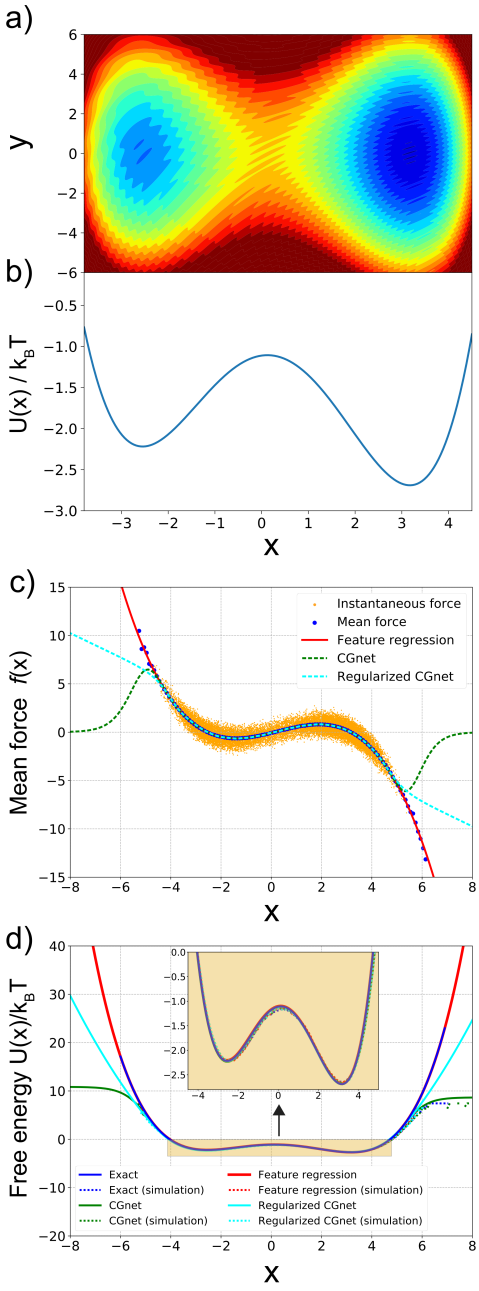


Figure 3: Machine-learned coarse-graining of dynamics in a rugged 2D potential. (a) 2D potential used as toy system. (b) Exact free energy along x. c) Instantaneous forces and the learned mean forces using feature regression and CGnet models (regularized and unregularized) compared to the exact forces. The unit of the force is k_BT, with the unit of length equal to 1. d) Free energy (PMF) along x predicted using least feature regression, and CGnet models compared to the exact free energy. Free energies are also computed from histogramming simulation data directly, using the underlying 2D trajectory, or simulations run with the feature regression and CGnet models (dashed lines).

the unregularized CGnet, a similar procedure is performed, and the best hyper-parameters are selected as $D = 1, W = 120$. Note that the prediction error cannot become zero, but is bounded from below by the chosen CG scheme (Fig. 1, Eq. 11) – in this case by neglecting the y variable.

Fig. 3c,d shows the results of the predicted mean forces and free energies (potentials of mean force) in the x-direction. The instantaneous force fluctuates around the mean, but serves to accurately fit the exact mean force in the x range where sampling is abundant using both feature regression and CGnet (Fig. 3c). At the boundary where few samples are in the training data the predictors start to diverge from the exact mean force and free energy (Fig. 3c, d). This effect is more dramatic for the unregularized CGnet, in particular at large x values the CGnet makes an arbitrary prediction: here the force tends to zero. In the present example, reaching these states is highly improbable. However a CGnet simulation reaching this region can fail dramatically, as the simulation may continue to diffuse away from the low energy regime. As discussed above, this behavior can be avoided by adding a suitable prior energy that ensures that the free energy keeps increasing outside the training data, while not affecting the accuracy of the learned free energy within the training data (Fig. 3c, d). Note that the quantitative mismatch in the low-probability regimes is not important for equilibrium simulations.

The matching mean forces translate into matching free energies (potentials of mean force, Fig. 3d). Finally, we conduct simulations with the learned models and generate trajectories $\{x_t\}$ using Eq. (14). From these, free energies can be computed by

$$\tilde{U}(\mathbf{x}) = -k_B T \ln \tilde{p}_X(\mathbf{x}) \qquad (18)$$

where $\tilde{p}_X(\mathbf{x})$ is a histogram estimate of the probability density of $\mathbf{x}$ in the simulation trajectories. As shown in Fig. 3d, free energies agree well in the x range that has significant equilibrium probability.

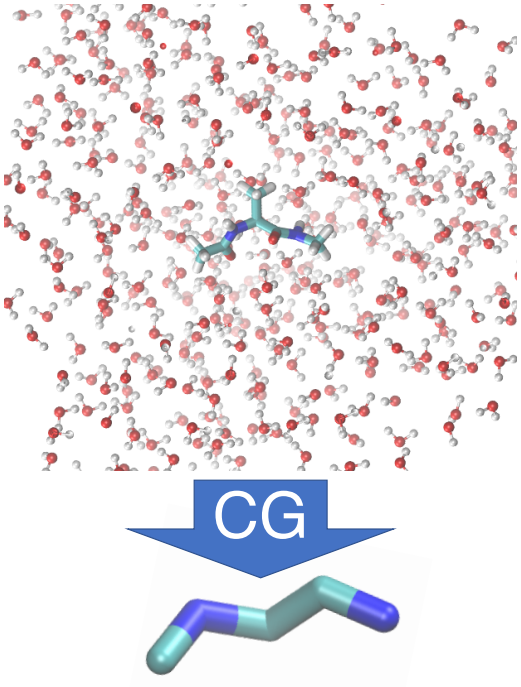


Figure 4: Mapping of alanine dipeptide from an all-atom solvated model (top) to a CG model consisting of the five central backbone atoms (bottom).

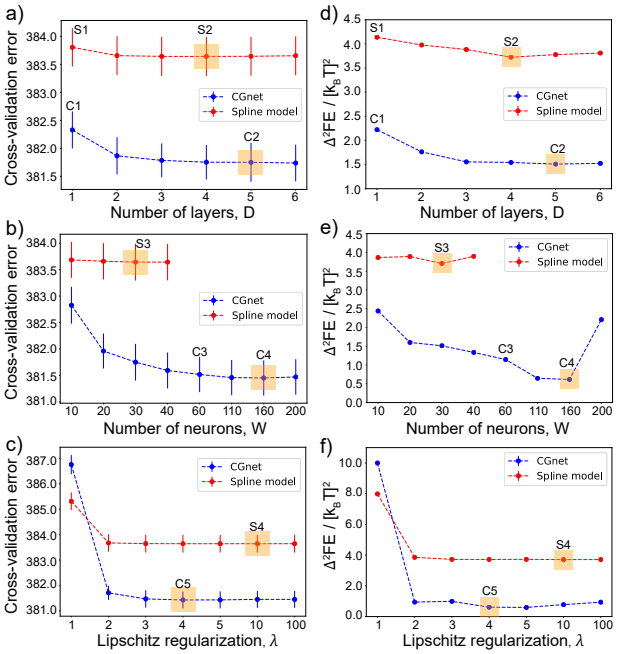


Figure 5: (a), (b), (c) Cross-validated force matching error in $[kcal/(mol{\cdot}\mathring{A})]^2$ for the selection of the optimum structure of the network, and (d), (e), (f) difference between the two-dimensional free energy surfaces obtained from the CG models and from the reference all-atom simulations (see Fig. 6) for the regularized CGnet and the spline model of alanine dipeptide. (a) Selection of the number of layers, D. (b) Selection of the number of neurons per layer, W. (c) Selection of the Lipschitz regularization strength, λ. The selected hyper-parameters, corresponding to the smallest cross-validation error are highlighted by orange boxes. Blue dashed lines represent the regularized CGnet, red dashed lines represent the spline model, vertical bars represent the standard error of the mean. Panels (d), (e), and (f) show the difference between the reference all-atom free energy surface and the free energy surfaces corresponding to the choices of hyper-parameters indicated in panels (a), (b), and (c) as (C1, C2, C3, C4, C5) for CGnet, and as (S1, S2, S3, S4) for the spline model.

Coarse-graining of alanine dipeptide in water

We now demonstrate CGnets on the coarse-graining of an all-atom MD simulation of alanine dipeptide in explicit solvent at $T = 300K$ to a simple model with 5 CG particles located at the five central backbone atoms of the molecule (Fig. 4). One trajectory of length 1 microsecond was generated using the simulation setup described in[74], coordinates and forces were saved every picosecond, giving rise to one million data points. The CG model has no solvent, therefore the CG procedure must learn the solvation free energy for all CG configurations.

We compare two different CG models. The first model, called "spline model", uses the state-of the art approach established in MD coarse-graining[11,49,59]: to express the CG potential as a sum of few-body interaction terms, similar as in classical MD forcefields. The most flexible amongst these approaches is to fit one-dimensional splines for each of the pairwise distance, angle and dihedral terms in order to parametrize two-, three- and four-body interactions[75]. In order to ensure a consistent comparison, we represent 1D splines with neural networks that map from a single input feature (pairwise distance, angle or dihedral) to a single free energy term, resulting in the spline model network shown in Fig. 2c. We use the same regularization and baseline energy for spline model networks and CGnets.

The second model uses a regularized multi-body CGnet, i.e., a fully connected neural network shown in Fig. 2b to approximate the CG free energy. The comparison of the results from the two models allows us to evaluate the importance of multi-body interactions that are cap-

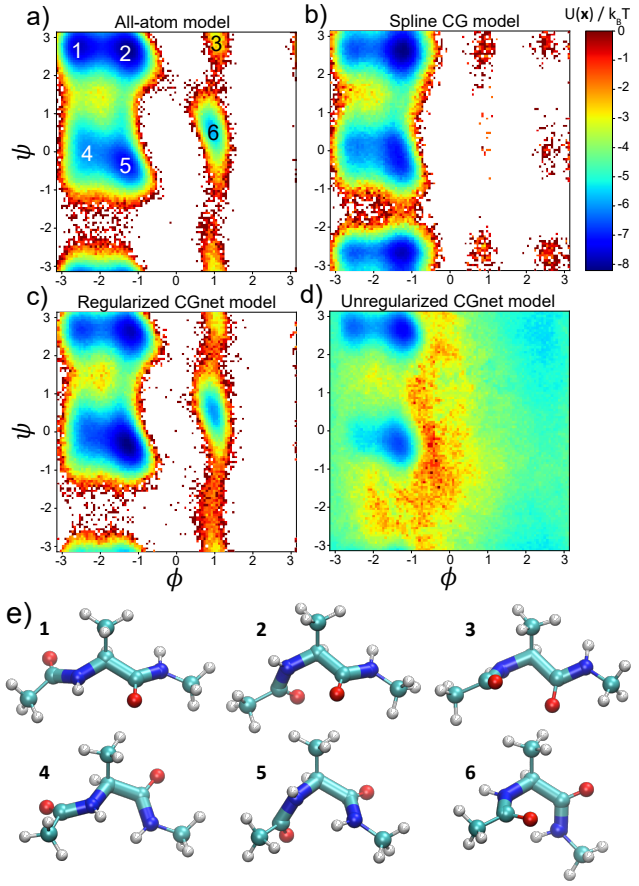


Figure 6: Free energy profiles and simulated structures of alanine dipeptide using all-atom and machine-learned coarse-grained models. (a)Reference free energy as a function of the dihedral angles, as obtained from direct histogram estimation from all-atom simulation. (b) Standard coarse-grained model using a sum of splines of individual internal coordinates. (c) Regularized CGnet as proposed here. (d) Unregularized CGnet. (e) Representative structures in the six free energy minima, from atomistic simulation (ball-and-stick representation) and regularized CGnet simulation (licorice representation).

tured by the CGnet but are generally absent in CG models that use interaction terms involving a few atoms only.

The hyper-parameters for both models consist of the number of layers (depth, D), the number of neurons per layer (width, W) of the network, and the Lipschitz regularization strength (λ)[68], and are optimized by a three-stage cross-validation. In the first stage, we find the optimal D at fixed $W = 30$ and $\lambda = \infty$ (no Lipschitz regularization), subsequently we choose W at the optimal D, and λ at the optimal W, D. This results in $D = 5$, $W = 160$, and $\lambda = 4.0$ for CGnet, and $D = 4$, $W = 30$ (for each feature), and $\lambda = 10.0$ for the spline model (Fig. 5). The cross-validation error of CGnet is significantly lower than the cross-validation error of the spline model (Fig. 5a-c). We point out that the cross-validation error cannot become zero, but is bounded from below by the chosen CG scheme (Fig. 1, Eq. 11) – in this case by coarse-graining all solvent molecules and all solute atoms except the five central backbone atoms away. Hence, the absolute numbers of the cross-validation error in Fig. 5a-c are not meaningful, only differences matter.

CG MD simulations are generated for the selected models by iterating Eq. (14). For each model, one hundred independent simulations starting from structures sampled randomly from the atomistic simulation are performed for 1 million steps each, and the aggregated data are used to produce the free energy as a function of the dihedral coordinates. Fig. 6 compares the free energy computed via (18) from the underlying atomistic MD simulations and the free energy resulting from the selected CG models. Only the regularized CGnet model can correctly reproduce the position of the all main free energy minima (Fig. 6a, c). On the contrary, the spline model is not able to capture the shallow minima corresponding to positive values of the dihedral angle ϕ, and introduces several spurious minima (Fig. 6b). This comparison confirms that selecting CG models by minimal mean force prediction error achieves models that are better from a physical viewpoint.

As an *a posteriori* analysis of the results we have performed MD simulation for the CG models corresponding to different choices of hyper-parameters, both for the spline model and CGnet. For each choice of hyper-parameters, we have computed the difference between the free energy as a function of the dihedral angles resulting from the CG simulations and the one from the all-atom models. Differences in free energy were estimated by discretizing the space spanned by the two dihedral angles and computing the mean square difference on all bins. The difference between a given model and CGnet was computed by shifting the free energy of CGnet by a constant

value that minimizes the overall mean square difference. The free energy difference for the spline models is always significantly larger than for the CGnet models (Fig. 5d-f). Interestingly, the minima in the difference in free energy correspond to the minima in the cross-validation curves reported in Fig. 5a-c, and the optimal values of hyper-parameters selected by cross-validation yield the absolute minimum in the free energy difference (indicated in Fig. 5f as C5 for CGnet and S4 for the spline model). This point is illustrated more explicitly in the SI (Section E, Figs. S4, S5), and demonstrates that the cross-validation error of different models are correlated with errors in approximating the two-dimensional free energy surface of alanine dipeptide.

For the CGnet, regularization is extremely important: without regularization the free energy only matches near the most pronounced minima and unphysical structures are sampled outside (Fig. 6d and SI Section D). With regularization, these unphysical regimes are avoided, all sampled structures appear chemically valid (Fig. 6e) and the distributions of bonds and angles follow those in the atomistic simulations (SI Section D, Fig. S3).

Coarse-graining of Chignolin folding/unfolding in water

Finally, we test the CGnet on a much more challenging problem: the folding/unfolding dynamics of the polypeptide Chignolin in water. Chignolin consists of 10 amino acids plus termini and exhibits a clear folding/unfolding transition. The all-atom model contains 1881 water molecules, salt ions and the Chignolin molecule, resulting in nearly 6000 atoms. To focus on the folding/unfolding transition, data was generated at the melting temperature 350 K, mimicking the setup used for the Anton supercomputer simulation in[4]. To obtain a well-converged ground truth, we generated 3742 short MD simulations with an aggregate length of 187.2 μs on GPUgrid[9] using the ACEMD program[5]. The free energy landscape is computed on the two collective variables describing the slowest processes, computed by the TICA method[17]. Since

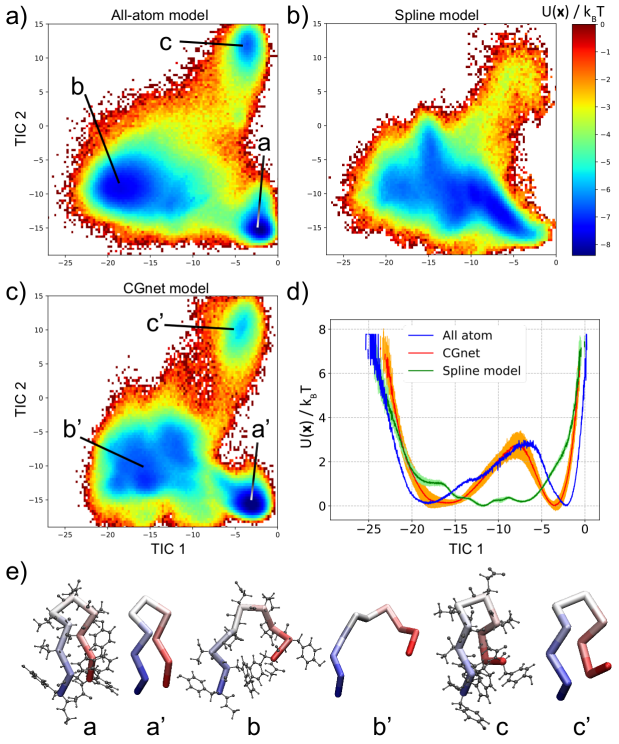


Figure 7: Free energy landscape of Chignolin for the different models. (a) The free energy as obtained from all-atom simulation, as a function of the first two TICA coordinates. (b) The free energy as obtained from the spline model, as a function of the same two coordinates used in the all-atom model. (c) The free energy as obtained from CGnet, as a function of the same two coordinates. (d) Comparison of the one dimensional free energy as a function of the first TICA coordinate (corresponding to the folding/unfolding transition) for the three models: all-atom (blue), spline (green), and CGnet (red). (e) Representative Chignolin configurations in the three minima from all-atom simulation (a, b, c) and CGnet (a', b', c').

the individual MD simulations are too short to reach equilibrium, the equilibrium distribution was recovered by reweighting all data using a Markov state model[12]. See SI for details on the MD simulation and Markov model analysis.

Fig. 7a shows the free energy as a function of the first two TICA coordinates. Three minima are clearly identifiable on this free energy landscape: states a (folded), b (unfolded) and c (partially misfolded), ordered alphabetically from most to least populated. Representative configurations in these minima as shown in Fig. 7e. As a result, the first TICA mode is a folding-unfolding coordinate, while the second is a misfolding coordinate.

Using a regularized CGnet, we coarse-grain the 6000-atom system to 10 CG beads representing the α-carbons of Chignolin. Thus, not only the polypeptide is coarse-grained, but also the solvation free energy is implicitly included in the CG model. Similar to what was done for alanine dipeptide, roto-translational invariance of the energy was implemented by using a CGnet featurization layer that maps the C_α Cartesian coordinates to all pairwise distances between CG beads, all angles defined by three adjacent CG beads, and the *cos* and *sin* of all the dihedral angles defined by four CG adjacent beads. The regularizing baseline energy includes a harmonic term for each bond and angle, and an excluded volume term for each pairwise distance between CG particles that are separated by more than two bonds.

Similar to the case of alanine dipeptide, a classical few-body spline model was defined for comparison whose CG potential is a sum of bonded and non-bonded terms, where each term is a nonlinear function of a single feature (pairwise distances, angles, dihedrals).

Both CGnet and spline model are optimized through a five-stage cross-validation search for the hyper-parameters, in the following order: Depth D, Width W, exponent of the excluded volume term c, radius of the excluded volume term σ, and Lipschitz regularization strength λ. The results of the cross-validation are shown in Fig. S8. This optimization resulted in the hyper-parameter values $D = 5$, $W = 250$, $c = 6$, $\sigma = 5.5$ and $\lambda = 4.0$. For the spline model, the optimal values of the hyper-parameters are $D = 3$, $W = 12$ (for each feature), $c = 10$, $\sigma = 4.0$, and $\lambda = 5.0$ (Fig. S8). The potential resulting from CGnet and the spline model is then used to run long simulations with Eq. (14). One hundred simulations of 1 million steps each were generated using randomly sampled configurations from the training data as starting points. For comparison, the aggregated data are projected on the TICA coordinates obtained from all-atom simulations and free energy landscapes are computed directly using Eq. (18) (Fig. 7b, c). For a more quantitative comparison, the free energies are also reported along the first TICA coordinate that indicates folding / unfolding (Fig. 7d).

These figures clearly show that the spline model cannot reproduce the folding/unfolding dynamics of Chignolin, as the folded and unfolded states are not well defined (Fig. 7b, d). On the contrary, CGnet not only can consistently fold and unfold the protein but also correctly identifies three well defined minima: the folded (a'), unfolded (b'), and partially misfolded (c') ensembles corresponding to the minima a, b, and c in the all-atom fully solvated model (Fig. 7c,d). Representative structures in the three minima are shown in Fig. 7e: the structures obtained from the CGnet simulations are remarkably similar to the ones obtained in the all-atom simulations. These results reinforce what has been already observed for alanine dipeptide above: the multi-body interactions captured by CGnet are essentialy for correct reproduction of the free energy landscape for the protein Chignolin. The absence of such interactions in the spline model dramatically alters the corresponding free energy landscape to the point that the model can not reproduce the folding/unfolding behavior of the protein.

Conclusions

Here we have formulated coarse-graining based on the force-matching principle as a machine learning method. An important consequence of this formulation is that coarse-graining is a supervised learning problem whose loss function can be decomposed into the standard terms of statistical estimator theory: Bias, Variance and Noise. These terms have well-defined physical meanings and can be used in conjunction with cross-validation in order to select model hyper-parameters and rank the quality of different coarse-graining models.

We have also introduced CGnets, a class of neural networks that can be trained with the force matching principle and can encode all physically relevant invariances and constraints: (1) invariance of the free energy and mean force with respect to translation of the molecule, (2) invariance of the free energy and equivariance of the mean force with respect to rotation of the

molecule, (3) the mean force is a conservative force field generated by the free energy, and (4) a prior energy can be applied in order to prevent the simulations with CGnets to diverge into unphysical state space regions outside the training data, such as states with overstretched bonds or clashing atoms. Future CGnets may include additional invariances, such as permutational invariance of identical CG particles, e.g. permutation of identical particles in symmetric rings.

The results presented above show that CGnet can be used to define effective energies for CG models that optimally reproduce the equilibrium distribution of a target atomistic model. CGnet provides a better approximation than functional forms commonly used for CG models as it automatically includes multi-body effects and non-linearities. The work presented here provides a proof of principle for this approach on relatively small solutes, but already demonstrates that the complex solvation free energy involved in the folding/unfolding of a polypeptide such as Chignolin can be encoded in a CGnet consisting of only the C_α atoms. The extension to larger and more complex molecules presents additional challenges and may require to include additional terms to enforce physical constraints.

Additionally, the CG model considered here is designed *ad hoc* for a specific molecule and is not transferable to the study of different systems. Transferability remains an outstanding issue in the design of coarse grained models[11] and its requirement may decrease the ability to reproduce faithfully properties of specific systems[49,81–84]. In principle, transferable potentials can be obtained by designing input features for CGnet imposing a dependence of the energy function on the CG particle types and their environment[82], similarly to what is done in the learning of potential energy functions from quantum mechanics data (see e.g.[20,24,27,33,66]). This approach may be able to define transferable functions if enough data are used in the training[27,33]. We leave the investigation on the trade-off between transferability and accuracy for future studies.

It is also important to note that the formulation used here to define an optimal CG potential aims at reproducing structural properties of the system, but it does not determine the equations for its dynamical evolution. If one is interested in designing CG models that can reproduce molecular dynamical mechanisms, e.g. to reproduce the slow dynamical processes of the fine-grained model, alternative approaches need to be investigated.

Acknowledgement We thank Alex Kluber, Justin Chen, Lorenzo Boninsegna, Eugen Hruska, and Feliks Nüske for comments on the manuscript. This work was supported by the National Science Foundation (CHE-1265929, CHE-1738990, and PHY-1427654), the Welch Foundation (C-1570), the MATH+ excellence cluster (AA1-6, EF1-2), the Deutsche Forschungsgemeinschaft (SFB 1114/C03, SFB 958/A04, TRR 186/A12), the European Commission (ERC CoG 772230 "ScaleCell"), the Einstein Foundation Berlin (Einstein Visiting Fellowship to CC), and the Alexander von Humboldt foundation (Postdoctoral fellowship to SO). Simulations have been performed on the computer clusters of the Center for Research Computing at Rice University, supported in part by the Big-Data Private-Cloud Research Cyberinfrastructure MRI-award (NSF grant CNS-1338099), and on the clusters of the Department of Mathematics and Computer Science at Freie Universität, Berlin. GDF acknowledges support from MINECO (Unidad de Excelencia María de Maeztu MDM-2014-0370 and BIO2017-82628-P) and FEDER. This project has received funding from the European Union's Horizon 2020 research and innovation programme under grant agreement No 675451 (CompBioMed project). We thank the GPUGRID donors for their compute time.

Supporting Information Available

The following files are available free of charge. Supporting Information is available providing:

- A derivation of equation (6)
- Cross-validation for all the models pre-

sented in the manuscript

- Additional details on the training of the models
- Distribution of bonds and angles for the different models of alanine dipeptide
- Changes in the free energy of alanine dipeptide with different hyper-parameters
- Energy decomposition for the CGnet model of alanine dipeptide
- Details on Chignolin setup and simulation
- Markov State Model analysis of Chignolin all-atom simulations

References

(1) Lindorff-Larsen, K.; Piana, S.; Dror, R. O.; Shaw, D. E. How Fast-Folding Proteins Fold. *Science* **2011**, *334*, 517–520.

(2) Buch, I.; Harvey, M. J.; Giorgino, T.; Anderson, D. P.; De Fabritiis, G. High-throughput all-atom molecular dynamics simulations using distributed computing. *J. Chem. Inf. Model.* **2010**, *50*, 397–403.

(3) Shirts, M.; Pande, V. S. Screen Savers of the World Unite! *Science* **2000**, *290*, 1903–1904.

(4) Dror, R. O.; Pan, A. C.; Arlow, D. H.; Borhani, D. W.; Maragakis, P.; Shan, Y.; Xu, H.; Shaw, D. E. Pathway and mechanism of drug binding to G-protein-coupled receptors. *Proc. Natl. Acad. Sci. USA* **2011**, *108*, 13118–13123.

(5) Shukla, D.; Meng, Y.; Roux, B.; Pande, V. S. Activation pathway of Src kinase reveals intermediate states as targets for drug design. *Nat. Commun.* **2014**, *5*, 3397.

(6) Plattner, N.; Noé, F. Protein conformational plasticity and complex ligand binding kinetics explored by atomistic simulations and Markov models. *Nat. Commun.* **2015**, *6*, 7653.

(7) Plattner, N.; Doerr, S.; Fabritiis, G. D.; Noé, F. Protein-protein association and binding mechanism resolved in atomic detail. *Nat. Chem.* **2017**, *9*, 1005–1011.

(8) Paul, F.; Wehmeyer, C.; Abualrous, E. T.; Wu, H.; Crabtree, M. D.; Schöneberg, J.; Clarke, J.; Freund, C.; Weikl, T. R.; Noé, F. Protein-ligand kinetics on the seconds timescale from atomistic simulations. *Nat. Commun.* **2017**, *8*, 1095.

(9) Clementi, C. Coarse-grained models of protein folding: Toy-models or predictive tools? *Curr. Opin. Struct. Biol.* **2008**, *18*, 10–15.

(10) Saunders, M. G.; Voth, G. A. Coarse-Graining Methods for Computational Biology. *Annu. Rev. Biophys.* **2013**, *42*, 73–93.

(11) Noid, W. G. Perspective: Coarse-grained models for biomolecular systems. *J. Chem. Phys.* **2013**, *139*, 090901.

(12) Matysiak, S.; Clementi, C. Optimal Combination of Theory and Experiment for the Characterization of the Protein Folding Landscape of S6: How Far Can a Minimalist Model Go? *J. Mol. Biol.* **2004**, *343*, 235–248.

(13) Matysiak, S.; Clementi, C. Minimalist protein model as a diagnostic tool for misfolding and aggregation. *J. Mol. Biol.* **2006**, *363*, 297–308.

(14) Chen, J.; Chen, J.; Pinamonti, G.; Clementi, C. Learning Effective Molecular Models from Experimental Observables. *J. Chem. Theory Comput.* **2018**, *14*, 3849–3858.

(15) Mardt, A.; Pasquali, L.; Wu, H.; Noé, F. VAMPnets: Deep learning of molecular kinetics. *Nat. Commun.* **2018**, *9*, 5.

(16) Wu, H.; Mardt, A.; Pasquali, L.; Noé, F. Deep Generative Markov State Models. *NIPS (in press). Preprint: arXiv:1805.07601* **2018**,

(17) Wehmeyer, C.; Noé, F. Time-lagged autoencoders: Deep learning of slow collective variables for molecular kinetics. *J. Chem. Phys.* **2018**, *148*, 241703.

(18) Hernández, C. X.; Wayment-Steele, H. K.; Sultan, M. M.; Husic, B. E.; Pande, V. S. Variational Encoding of Complex Dynamics. *arXiv:1711.08576* **2017**,

(19) Ribeiro, J. M. L.; Bravo, P.; Wang, Y.; Tiwary, P. Reweighted autoencoded variational Bayes for enhanced sampling (RAVE). *J. Chem. Phys.* **2018**, *149*, 072301.

(20) Behler, J.; Parrinello, M. Generalized Neural-Network Representation of High-Dimensional Potential-Energy Surfaces. *Phys. Rev. Lett.* **2007**, *98*, 146401.

(21) Bartók, A. P.; Payne, M. C.; Kondor, R.; Csányi, G. Gaussian Approximation Potentials: The Accuracy of Quantum Mechanics, without the Electrons. *Phys. Rev. Lett.* **2010**, *104*, 136403.

(22) Rupp, M.; Tkatchenko, A.; Müller, K.-R.; von Lilienfeld, O. A. Fast and Accurate Modeling of Molecular Atomization Energies with Machine Learning. *Phys. Rev. Lett.* **2012**, *108*, 058301.

(23) Bartók, A. P.; Gillan, M. J.; Manby, F. R.; Csányi, G. Machine-learning approach for one- and two-body corrections to density functional theory: Applications to molecular and condensed water. *Phys. Rev. B* **2013**, *88*, 054104.

(24) Smith, J. S.; Isayev, O.; Roitberg, A. E. ANI-1: an extensible neural network potential with DFT accuracy at force field computational cost. *Chem. Sci.* **2017**, *8*, 3192–3203.

(25) Chmiela, S.; Tkatchenko, A.; Sauceda, H. E.; Poltavsky, I.; Schütt, K. T.; Müller, K.-R. Machine learning of accurate energy-conserving molecular force fields. *Sci. Adv.* **2017**, *3*, e1603015.

(26) Bartók, A. P.; De, S.; Poelking, C.; Bernstein, N.; Kermode, J. R.; Csányi, G.; Ceriotti, M. Machine learning unifies the modeling of materials and molecules. *Sci. Adv.* **2017**, *3*, e1701816.

(27) Schütt, K. T.; Arbabzadah, F.; Chmiela, S.; Müller, K. R.; Tkatchenko, A. Quantum-chemical insights from deep tensor neural networks. *Nat. Commun.* **2017**, *8*, 13890.

(28) Smith, J. S.; Nebgen, B.; Lubbers, N.; Isayev, O.; Roitberg, A. E. Less is more: Sampling chemical space with active learning. *J. Chem. Phys.* **2018**, *148*, 241733.

(29) Schütt, K. T.; Sauceda, H. E.; Kindermans, P.-J.; Tkatchenko, A.; Müller, K.-R. SchNet - A deep learning architecture for molecules and materials. *J. Chem. Phys.* **2018**, *148*, 241722.

(30) Grisafi, A.; Wilkins, D. M.; Csányi, G.; Ceriotti, M. Symmetry-Adapted Machine Learning for Tensorial Properties of Atomistic Systems. *Phys. Rev. Lett.* **2018**, *120*, 036002.

(31) Imbalzano, G.; Anelli, A.; Giofré, D.; Klees, S.; Behler, J.; Ceriotti, M. Automatic selection of atomic fingerprints and reference configurations for machine-learning potentials. *J. Chem. Phys.* **2018**, *148*, 241730.

(32) Nguyen, T. T.; Székely, E.; Imbalzano, G.; Behler, J.; Csányi, G.; Ceriotti, M.; Götz, A. W.; Paesani, F. Comparison of permutationally invariant polynomials, neural networks, and Gaussian approximation potentials in representing water interactions through many-body expansions. *J. Chem. Phys.* **2018**, *148*, 241725.

(33) Zhang, L.; Han, J.; Wang, H.; Saidi, W. A.; Car, R.; E, W. End-to-end Symmetry Preserving Inter-atomic Potential Energy Model for Finite and Extended Systems. *arXiv:1805.09003* **2018**,

(34) Zhang, L.; Han, J.; Wang, H.; Car, R.; E, W. Deep potential molecular dynamics: a scalable model with the accuracy of quantum mechanics. *Phys. Rev. Lett.* **2018**, *120*, 143001.

(35) Bereau, T.; DiStasio, R. A.; Tkatchenko, A.; Lilienfeld, O. A. V. Non-covalent interactions across organic and biological subsets of chemical space: Physics-based potentials parametrized from machine learning. *J. Chem. Phys.* **2018**, *148*, 241706.

(36) Wang, H.; Yang, W. Toward Building Protein Force Fields by Residue-Based Systematic Molecular Fragmentation and Neural Network. *J. Chem. Theory Comput.* **2019**, *15*, 1409–1417.

(37) John, S. T.; Csányi, G. Many-Body Coarse-Grained Interactions Using Gaussian Approximation Potentials. *J. Phys. Chem. B* **2017**, *121*, 10934–10949.

(38) Zhang, L.; Han, J.; Wang, H.; Car, R.; E, W. DeePCG: constructing coarse-grained models via deep neural networks. *arXiv:1802.08549* **2018**,

(39) Chan, H.; Cherukara, M. J.; Narayanan, B.; Loeffler, T. D.; Benmore, C.; Gray, S. K.; Sankaranarayanan, S. K. R. S. Machine learning coarse grained models for water. *Nat. Commun.* **2019**, *10*, 379.

(40) Lemke, T.; Peter, C. Neural Network Based Prediction of Conformational Free Energies - A New Route toward Coarse-Grained Simulation Models. *J. Chem. Theory Comput.* **2017**, *13*, 6213–6221.

(41) Bejagam, K. K.; Singh, S.; An, Y.; Deshmukh, S. A. Machine-Learned Coarse-Grained Models. *J. Phys. Chem. Lett.* **2018**, *9*, 4667–4672, PMID: 30024761.

(42) Stecher, T.; Bernstein, N.; Csányi, G. Free Energy Surface Reconstruction from Umbrella Samples Using Gaussian Process Regression. *J. Chem. Theory Comput.* **2014**, *10*, 4079–4097.

(43) Schneider, E.; Dai, L.; Topper, R. Q.; Drechsel-Grau, C.; Tuckerman, M. E. Stochastic neural network approach for learning high-dimensional free energy surfaces. *Phys. Rev. Lett.* **2017**, *119*, 150601.

(44) Sidky, H.; Whitmer, J. K. Learning free energy landscapes using artificial neural networks. *J. Chem. Phys.* **2018**, *148*, 104111.

(45) Lyubartsev, A. P.; Laaksonen, A. Calculation of effective interaction potentials from radial distribution functions: A reverse Monte Carlo approach. *Phys. Rev. E* **1995**, *52*, 3730–3737.

(46) Müller-Plathe, F. Coarse-Graining in Polymer Simulation: From the Atomistic to the Mesoscopic Scale and Back. *ChemPhysChem* **2002**, *3*, 754–769.

(47) Praprotnik, M.; Site, L. D.; Kremer, K. Multiscale Simulation of Soft Matter: From Scale Bridging to Adaptive Resolution. *Ann. Rev. Phys. Chem.* **2008**, *59*, 545–571.

(48) Izvekov, S.; Voth, G. A. A Multiscale Coarse-Graining Method for Biomolecular Systems. *J. Phys. Chem. B* **2005**, *109*, 2469–2473.

(49) Wang, Y.; Noid, W. G.; Liu, P.; Voth, G. A. Effective force coarse-graining. *Phys. Chem. Chem. Phys.* **2009**, *11*, 2002.

(50) Shell, M. S. The relative entropy is fundamental to multiscale and inverse thermodynamic problems. *J. Phys. Chem.* **2008**, *129*, 144108.

(51) Clementi, C.; Nymeyer, H.; Onuchic, J. N. Topological and energetic factors: what determines the structural details of the transition state ensemble and "en-route" intermediates for protein folding? Investigation for small globular proteins. *J. Mol. Biol.* **2000**, *298*, 937–953.

(52) Nielsen, S. O.; Lopez, C. F.; Srinivas, G.; Klein, M. L. A coarse grain model for n-alkanes parameterized from surface tension data. *J. Chem. Phys.* **2003**, *119*, 7043–7049.

(53) Marrink, S. J.; de Vries, A. H.; Mark, A. E. Coarse Grained Model for Semiquantitative Lipid Simulations. *J. Phys. Chem. B* **2004**, *108*, 750–760.

(54) Davtyan, A.; Schafer, N. P.; Zheng, W.; Clementi, C.; Wolynes, P. G.; Papoian, G. A. AWSEM-MD: Protein Structure Prediction Using Coarse-Grained Physical Potentials and Bioinformatically Based Local Structure Biasing. *J. Phys. Chem. B* **2012**, *116*, 8494–8503.

(55) Voth, G. A. *Coarse-graining of condensed phase and biomolecular systems*; CRC press, 2008.

(56) Monticelli, L.; Kandasamy, S. K.; Periole, X.; Larson, R. G.; Tieleman, D. P.; Marrink, S.-J. The MARTINI Coarse-Grained Force Field: Extension to Proteins. *J. Chem. Theory Comput.* **2008**, *4*, 819–834.

(57) Sinitskiy, A. V.; Saunders, M. G.; Voth, G. A. Optimal number of coarse-grained sites in different components of large biomolecular complexes. *J. Phys. Chem. B* **2012**, *116*, 8363–8374.

(58) Boninsegna, L.; Banisch, R.; Clementi, C. A Data-Driven Perspective on the Hierarchical Assembly of Molecular Structures. *J. Chem. Theory Comput.* **2018**, *14*, 453–460.

(59) Noid, W. G.; Chu, J.-W.; Ayton, G. S.; Krishna, V.; Izvekov, S.; Voth, G. A.; Das, A.; Andersen, H. C. The multiscale coarse-graining method. I. A rigorous bridge between atomistic and coarse-grained models. *J. Chem. Phys.* **2008**, *128*, 244114.

(60) Rudzinski, J. F.; Noid, W. G. Coarse-graining entropy, forces, and structures. *J. Phys. Chem.* **2011**, *135*, 214101.

(61) Vapnik, V. N. An Overview of Statistical Learning Theory. *IEEE Trans. Neur. Net.* **1999**, *10*, 988–999.

(62) Devijver, P. A.; Kittler, J. *Pattern Recognition: A Statistical Approach*; Prentice-Hall, London, 1982.

(63) Kohavi, R. A study of cross-validation and bootstrap for accuracy estimation and model selection. Proceedings of the Fourteenth International Joint Conference on Artificial Intelligence San Mateo, CA. 1995; pp 1137–1143.

(64) Hornik, K. Approximation Capabilities of Multilayer Feedforward Networks. *Neural Networks* **1991**, *4*, 251–257.

(65) Hansen, K.; Montavon, G.; Biegler, F.; Fazli, S.; Rupp, M.; Scheffler, M.; Lilienfeld, O. A. V.; Tkatchenko, A.; Müller, K.-R. Assessment and validation of machine learning methods for predicting molecular atomization energies. *J. Chem. Theory Comput.* **2013**, *9*, 3404–3419.

(66) Bartók, A. P.; Kondor, R.; Csányi, G. On representing chemical environments. *Phys. Rev. B* **2013**, *87*, 184115.

(67) Chmiela, S.; Sauceda, H. E.; Müller, K.-R.; Tkatchenko, A. Towards exact molecular dynamics simulations with machine-learned force fields. *Nature Commun.* **2018**, *9*, 3887.

(68) Gouk, H.; Frank, E.; Pfahringer, B.; Cree, M. Regularisation of Neural Networks by Enforcing Lipschitz Continuity. *arXiv:1804.04368* **2018**,

(69) Goodfellow, I.; Bengio, Y.; Courville, A. *Deep Learning*; MIT Press, 2016.

(70) Shapeev, A. V. Moment Tensor Potentials: a class of systematically improvable interatomic potentials. *Multiscale Model. Simul.* **2016**, *14*, 1153.

(71) Dolgirev, P. E.; Kruglov, I. A.; Oganov, A. R. Machine learning scheme for fast extraction of chemically interpretable interatomic potentials. *AIP Adv.* **2016**, *6*, 085318.

(72) Deringer, V. L.; Csányi, G. Machine learning based interatomic potential for amorphous carbon. *Phys. Rev. B* **2017**, *95*, 094203.

(1) Boninsegna, L.; Nüske, F.; Clementi, C. Sparse learning of stochastic dynamical equations. *J. Chem. Phys.* **2018**, *148*, 241723.

(74) Nüske, F.; Wu, H.; Wehmeyer, C.; Clementi, C.; Noé, F. Markov State Models from short non-Equilibrium Simulations - Analysis and Correction of Estimation Bias. *J. Chem. Phys.* **2017**, *146*, 094104.

(75) Dunn, N. J. H.; Lebold, K. M.; DeLyser, M. R.; Rudzinski, J. F.; Noid, W. BOCS: Bottom-up Open-source Coarse-graining Software. *J. Phys. Chem. B* **2017**, *122*, 3363–3377.

(4) Lindorff-Larsen, K.; Piana, S.; Dror, R. O.; Shaw, D. E. How fast-folding proteins fold. *Science* **2011**, *334*, 517–20.

(9) Buch, I.; Harvey, M. J.; Giorgino, T.; Anderson, D. P.; De Fabritiis, G. High-throughput all-atom molecular dynamics simulations using distributed computing. *J. Chem. Inf. Model.* **2010**, *50*, 397–403.

(5) Harvey, M. J.; Giupponi, G.; De Fabritiis, G. ACEMD: Accelerating biomolecular dynamics in the microsecond time scale. *J. Chem. Theory Comput.* **2009**, *5*, 1632–1639.

(17) Perez-Hernandez, G.; Paul, F.; Giorgino, T.; D Fabritiis, G.; Noé, F. Identification of slow molecular order parameters for Markov model construction. *J. Chem. Phys.* **2013**, *139*, 015102.

(12) Prinz, J.-H.; Wu, H.; Sarich, M.; Keller, B. G.; Senne, M.; Held, M.; Chodera, J. D.; Schütte, C.; Noé, F. Markov models of molecular kinetics: Generation and Validation. *J. Chem. Phys.* **2011**, *134*, 174105.

(81) Johnson, M. E.; Head-Gordon, T.; Louis, A. A. Representability problems for coarse-grained water potentials. *J. Chem. Phys.* **2007**, *126*, 144509.

(82) Mullinax, J. W.; Noid, W. G. Extended ensemble approach for deriving transferable coarse-grained potentials. *J. Chem. Phys.* **2009**, *131*, 104110.

(83) Thorpe, I. F.; Goldenberg, D. P.; Voth, G. A. Exploration of Transferability in Multiscale Coarse-Grained Peptide Models. *J. Phys. Chem. B* **2011**, *115*, 11911–11926.

(84) Allen, E. C.; Rutledge, G. C. Evaluating the transferability of coarse-grained, density-dependent implicit solvent models to mixtures and chains. *J. Chem. Phys.* **2009**, *130*, 034904.

Supplementary Material

Decomposition of the force matching error

The decomposition of the force matching error (4) can be achieved by adding and subtracting the mean force (5) and splitting the norm:

$$\begin{aligned}\chi^2\left[U(\mathbf{x})\right] &= \left\langle \left\langle \|\xi(\mathbf{F}(\mathbf{r})) - \mathbf{f}(\mathbf{x}) + \mathbf{f}(\mathbf{x}) + \nabla U(\mathbf{x})\|^2 \right\rangle_{\mathbf{r}|\mathbf{x}} \right\rangle_{\mathbf{x}} \\ &= \left\langle \left\langle \|\xi(\mathbf{F}(\mathbf{r})) - \mathbf{f}(\mathbf{x})\|^2 \right\rangle_{\mathbf{r}|\mathbf{x}} \right\rangle_{\mathbf{x}} + \left\langle \|\mathbf{f}(\mathbf{x}) + \nabla U(\mathbf{x})\|^2 \right\rangle_{\mathbf{x}} \\ &\quad +2 \left\langle \left\langle (\xi(\mathbf{F}(\mathbf{r})) - \mathbf{f}(\mathbf{x}))^\top (\mathbf{f}(\mathbf{x}) + \nabla U(\mathbf{x})) \right\rangle_{\mathbf{r}|\mathbf{x}} \right\rangle_{\mathbf{x}}.\end{aligned}$$

This expression is equivalent to Eq. (6). as the mixed term is zero:

$$\begin{aligned}&\left\langle \left\langle (\xi(\mathbf{F}(\mathbf{r})) - \mathbf{f}(\mathbf{x}))^\top (\mathbf{f}(\mathbf{x}) + \nabla U(\mathbf{x})) \right\rangle_{\mathbf{r}|\mathbf{x}} \right\rangle_{\mathbf{x}} \\ &= \left\langle \mathbf{f}(\mathbf{x})^\top \mathbf{f}(\mathbf{x}) \right\rangle_{\mathbf{x}} + \left\langle \mathbf{f}(\mathbf{x})^\top \nabla U(\mathbf{x}) \right\rangle_{\mathbf{x}} \\ &\quad - \left\langle \mathbf{f}(\mathbf{x})^\top \mathbf{f}(\mathbf{x}) \right\rangle_{\mathbf{x}} - \left\langle \mathbf{f}(\mathbf{x})^\top \nabla U(\mathbf{x}) \right\rangle_{\mathbf{x}} \\ &= 0\end{aligned}$$

The decomposition of the expected prediction error in the form of Eq. (11) can be achieved by adding and subtracting the mean estimator $\bar{\mathbf{f}}(\mathbf{X}) = \mathbb{E}\left[-\nabla U(\mathbf{X};\boldsymbol{\theta})\right]$:

$$\begin{aligned}\mathbb{E}\left[L(\boldsymbol{\theta};\mathbf{R})\right] &= \mathbb{E}_{\mathbf{R}|\mathbf{X}}\left[\|\mathbf{f}(\mathbf{X}) + \nabla U(\mathbf{X};\boldsymbol{\theta})\|_F^2\right] + \text{Noise} \\ &= \mathbb{E}\left[\left\| \underbrace{\left(\mathbf{f}(\mathbf{X}) - \bar{\mathbf{f}}(\mathbf{X})\right)}_{A} + \underbrace{\left(\bar{\mathbf{f}}(\mathbf{X}) + \nabla U(\mathbf{X};\boldsymbol{\theta})\right)}_{B} \right\|_F^2\right] + \text{Noise} \\ &= \mathbb{E}\left[\|A\|_F^2\right] + \mathbb{E}\left[\|B\|_F^2\right] + 2\mathbb{E}\left[\sum_{i,j} (A * B)_{i,j}\right] + \text{Noise},\end{aligned}$$

where $*$ is the element-wise product. We follow standard results for regression. For the mixed term we can use

$$\mathbb{E}\left[\sum_{i,j} (A * B)_{i,j}\right] = \sum_{i,j} \mathbb{E}\left[(A * B)_{i,j}\right] = \sum_{i,j} \left(\mathbb{E}\left[A * B\right]\right)_{i,j}$$

and this expectation value disappears:

$$\begin{aligned}\mathbb{E}\left[A * B\right] &= \mathbb{E}\left[\left(\mathbf{f}(\mathbf{X}) - \bar{\mathbf{f}}(\mathbf{X})\right) * \left(\bar{\mathbf{f}}(\mathbf{X}) + \nabla U(\mathbf{X};\boldsymbol{\theta})\right)\right] \\ &= \mathbb{E}\left[\mathbf{f}(\mathbf{X})\right] * \bar{\mathbf{f}}(\mathbf{X}) + \mathbb{E}\left[\mathbf{f}(\mathbf{X}) * \nabla U(\mathbf{X};\boldsymbol{\theta})\right] - \mathbb{E}\left[\bar{\mathbf{f}}(\mathbf{X}) * \bar{\mathbf{f}}(\mathbf{X})\right] - \bar{\mathbf{f}}(\mathbf{X}) * \mathbb{E}\left[\nabla U(\mathbf{X};\boldsymbol{\theta})\right] \\ &= \mathbf{f}(\mathbf{X}) * \bar{\mathbf{f}}(\mathbf{X}) - \mathbf{f}(\mathbf{X}) * \bar{\mathbf{f}}(\mathbf{X}) - \bar{\mathbf{f}}(\mathbf{X}) * \bar{\mathbf{f}}(\mathbf{X}) + \bar{\mathbf{f}}(\mathbf{X}) * \bar{\mathbf{f}}(\mathbf{X}) \\ &= 0.\end{aligned}$$

The remaining terms define bias and variance.

Cross-validation for the coarse-graining of the 2d toy model

We report here the results from cross-validation for the choice of hyper-parameters for the coarse-graining of the 2d toy model discussed in the main text.

The feature regression for the coarse-graining of the 2 dimensional toy model is performed with the twenty basis functions listed in Table S1 selected as features. Cross-validation is performed with the Stepwise Sparse Regressor introduced in[1]. The minimum cross-validation error is obtained when the first four functions are used as features, as shown in Fig. S1.

Table S1: Twenty elementary basis functions.

function ID	function, $f(x)$	function ID	function, $f(x)$
1	1	11	x^{10}
2	x	12	$sin(x)$
3	x^2	13	$cos(x)$
4	x^3	14	$sin(6x)$
5	x^4	15	$cos(6x)$
6	x^5	16	$sin(11x)$
7	x^6	17	$cos(11x)$
8	x^7	18	$tanh(10x)$
9	x^8	19	$tanh^2(10x)$
10	x^9	20	e^{-50x^2}

The results from the cross-validation of the CGnet for the toy 2 dimensional system are reported in Tables S2 and Fig. S1.

Table S2: Hyper-parameter optimization for unregularized CGnet of two-dimensional model system. D: network depth, W : network width. The unit of the cross-validation error is $(k_BT)^2$, with the unit of length equal to 1.

D ($W = 20$)	Cross-validation error
1	**0.3785 ± 0.0024**
2	0.5457 ± 0.0973
3	0.7339 ± 0.0298
4	0.5695 ± 0.0172
5	0.8543 ± 0.1227

W ($D = 1$)	Cross-validation error
5	0.5674 ± 0.0044
10	0.8762 ± 0.0048
20	0.3785 ± 0.0024
40	0.3729 ± 0.0017
60	0.3703 ± 0.0013
80	0.3682 ± 0.0013
100	0.3671 ± 0.0013
120	**0.3661 ± 0.0012**
150	0.3661 ± 0.0012

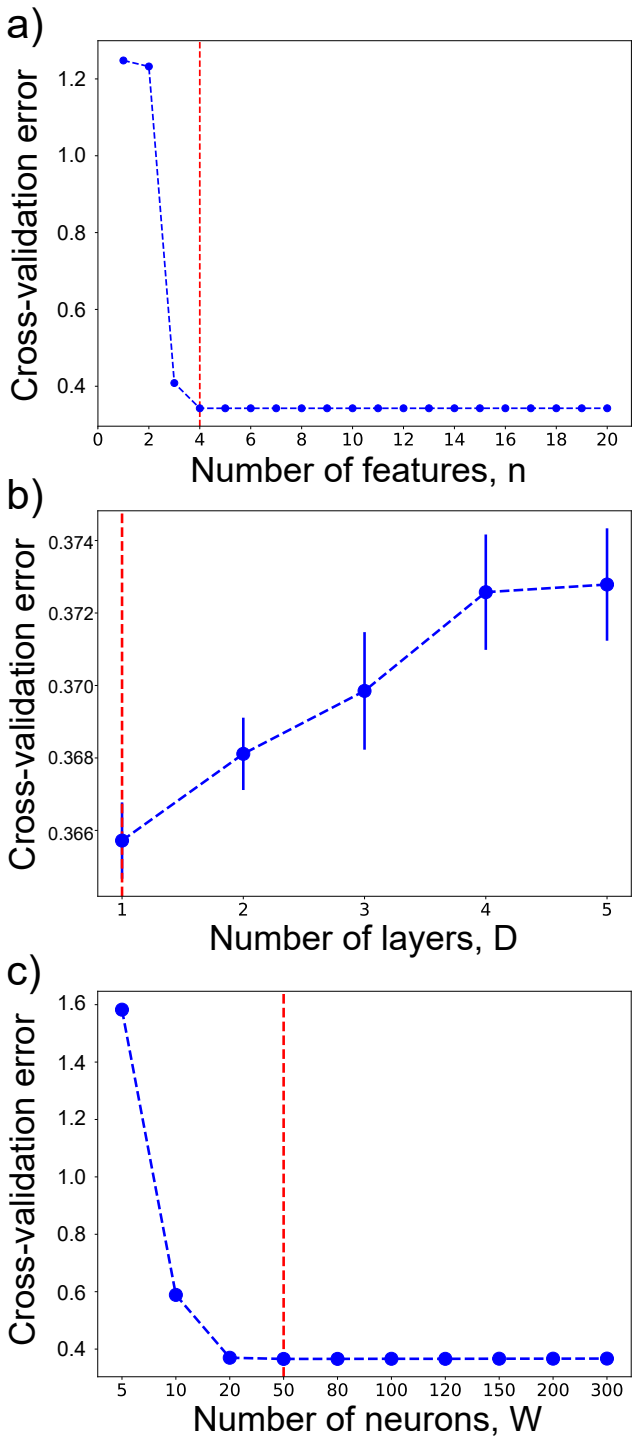


Figure S1: Model selection for CG model of 2D system using cross-validation. a) Choice of the set of feature functions for feature regression. b) First stage of regularized CGnet hyper-parameter selection: the optimal number of layers, D. c). Second stage of regularized CGnet hyperparameter selection: the optimal number of neurons per layer, W. Red dashed lines indicate the minimal cross-validation error. Error bars represent the standard error of the mean cross-validation error over five cross-validation folds, in panels a) and c) the error bars are invisible as they are smaller than the marker. The unit of the cross-validation error is $(k_BT)^2$, with the unit of length equal to 1.

Training CG models

Networks were optimized using the Adam adaptive stochastic gradient descent method [2] with default settings using the PyTorch program. The batch-size was 128 for the 2D model and 512 for alanine dipeptide. The convergence of the training error and validation error for the 2d toy model and alanine dipeptide is shown in Fig. S2 below.

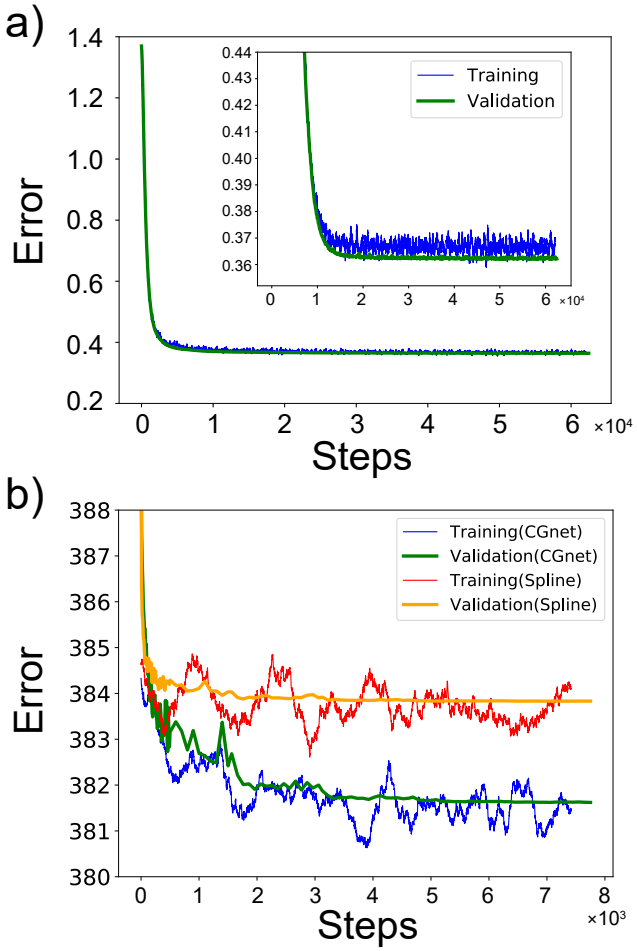


Figure S2: Training error and validation error for (a) the 2D model and (b) alanine dipeptide. In (a), the model is the regularized CGnet, in (b), the model is the regularized CGnet and the spline model, which is also regularized. All errors are averaged over 200000 points – for the training error this is done by averaging over the most recent batches, while the validation error is shown for a fixed validation set. Note that the hyper-parameter choices are made via cross-validation. The unit of the error is $(k_BT)^2$ in (a) and $[kcal/(mol\cdot\mathring{A})]^2$ in (b).

Distribution of bond distances and angles for the different models of alanine dipeptide

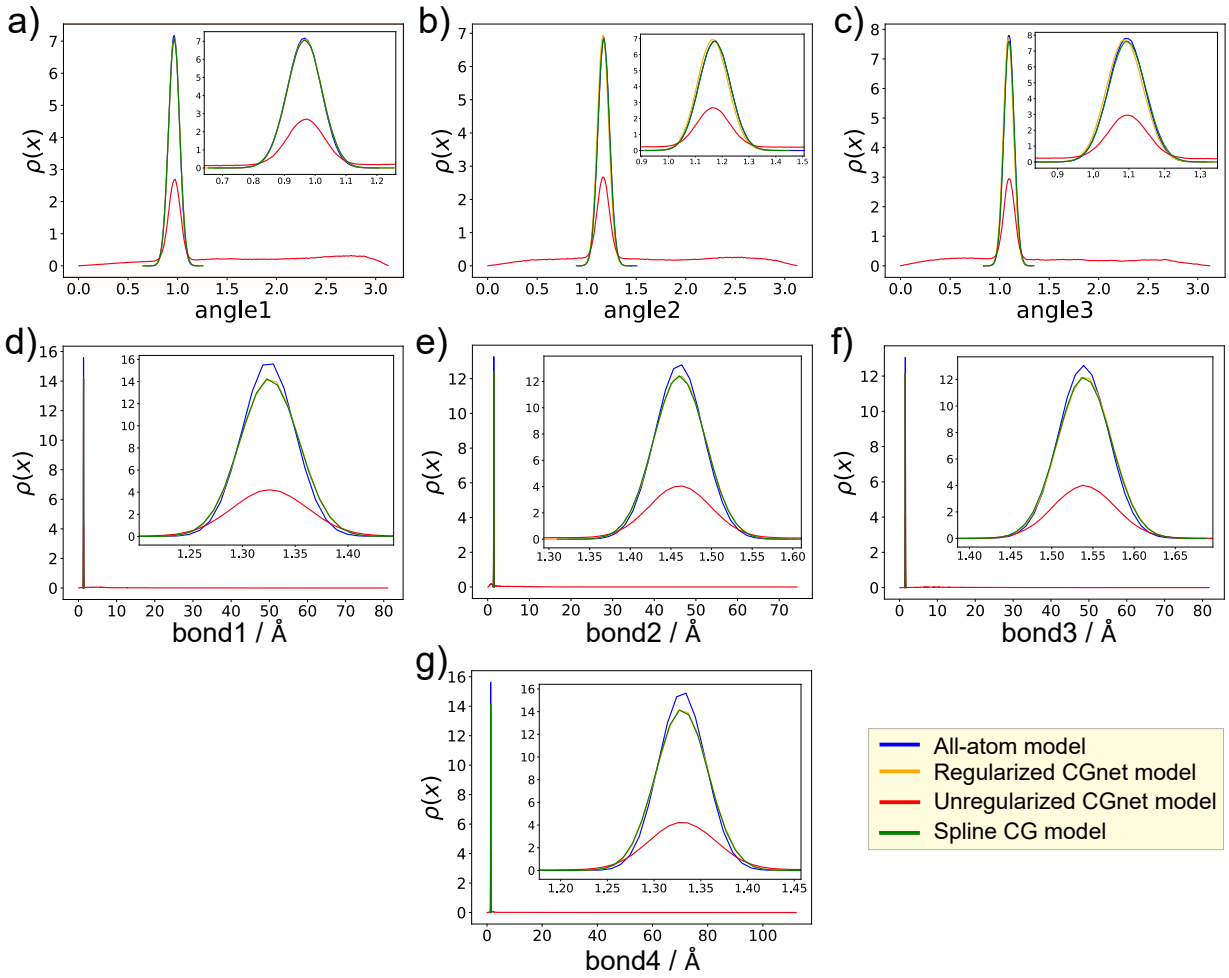


Figure S3: Probability density distribution for three angles a)- c), and four bonds d)-g) for the alanine dipeptide models. Each panel contains the distribution from four models: All-atom model (blue), regularized CGnet model (red), unregularized CGnet model (cyan), spline CG model (green). The distribution for regularized CGnet and spline model (with regularization) agree with the true all-atom one. The distribution for the unregularized CGnet has a wide range, which makes the distributions for the other models appear very narrow in d)-g). The insets in d)-g) present zoomed views of the distributions in the correct range.

Changes in the free energy of alanine dipeptide with different hyper-parameters

In order to show how the free energy is approximating the atomistic free energy as the hyper-parameters gradually reach the optimal values, we select five hyper-parameters for CGnet (C1, C2, C3, C4, C5) and four for the Spline model (S1, S2, S3, S4), as indicated in Fig. 5 in the manuscript. For each of these combinations of hyper-parameters, we report the corresponding two dimensional free energy profiles in Fig. S4 and Fig. S5 (in addition to the free energy profile for the global optima reported in Fig. 6). The figures show that as the hyper-parameters get closer to the optimal values the model free energy landscape becomes closer to the atomistic free energy landscape.

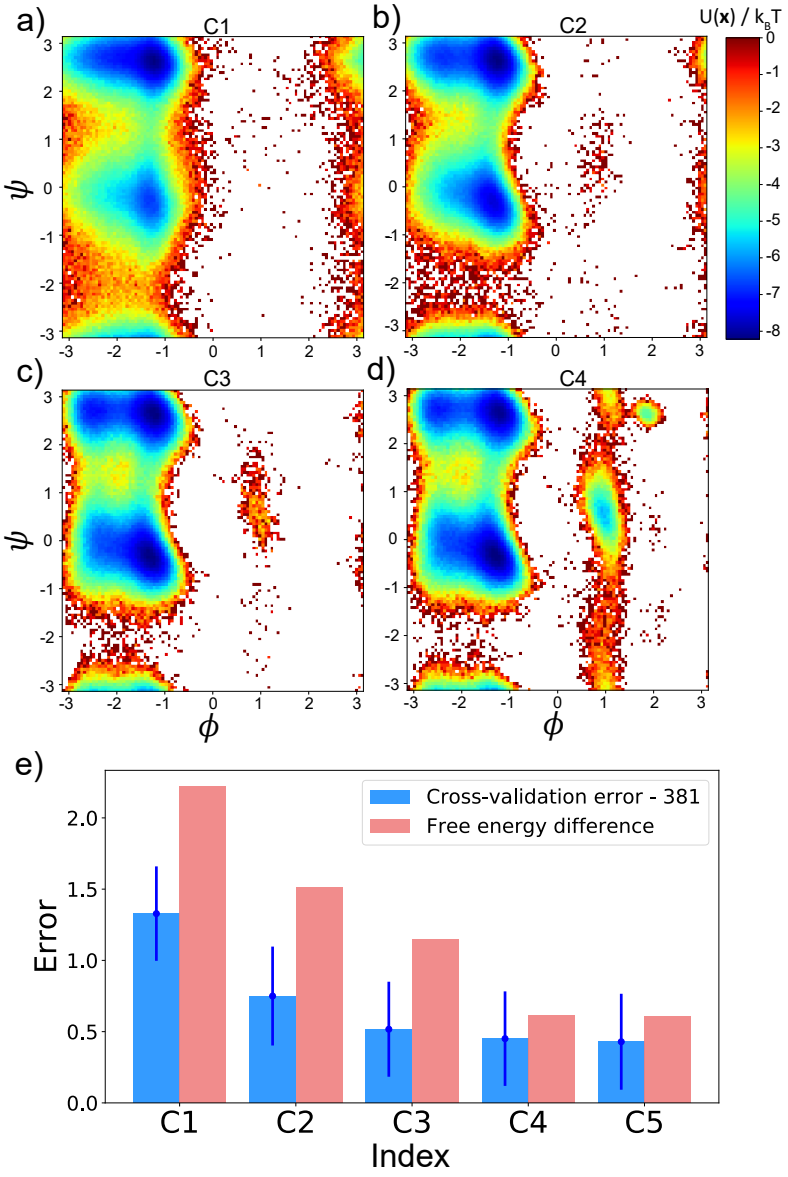


Figure S4: Comparison of the free energy profiles of CGnet models of alanine dipeptide with different choices of hyper-parameters. (a)-(d) Free energy profiles with hyperparameters corresponding to the combination indicated as C1, C2, C3, C4 in Fig. 5. The choice of hyperparameters C5 correspond to the global optimum and is reported in Fig. 6c. (e) Comparison between the cross validation error (in $[kcal/(mol{\cdot}\text{Å})]^2$) and mean square free energy difference (in $[k_BT]^2$) for the five selected hyperparameters. The value of 381 is subtracted from the cross validation error to obtain values in the similar range as the free energy differences.

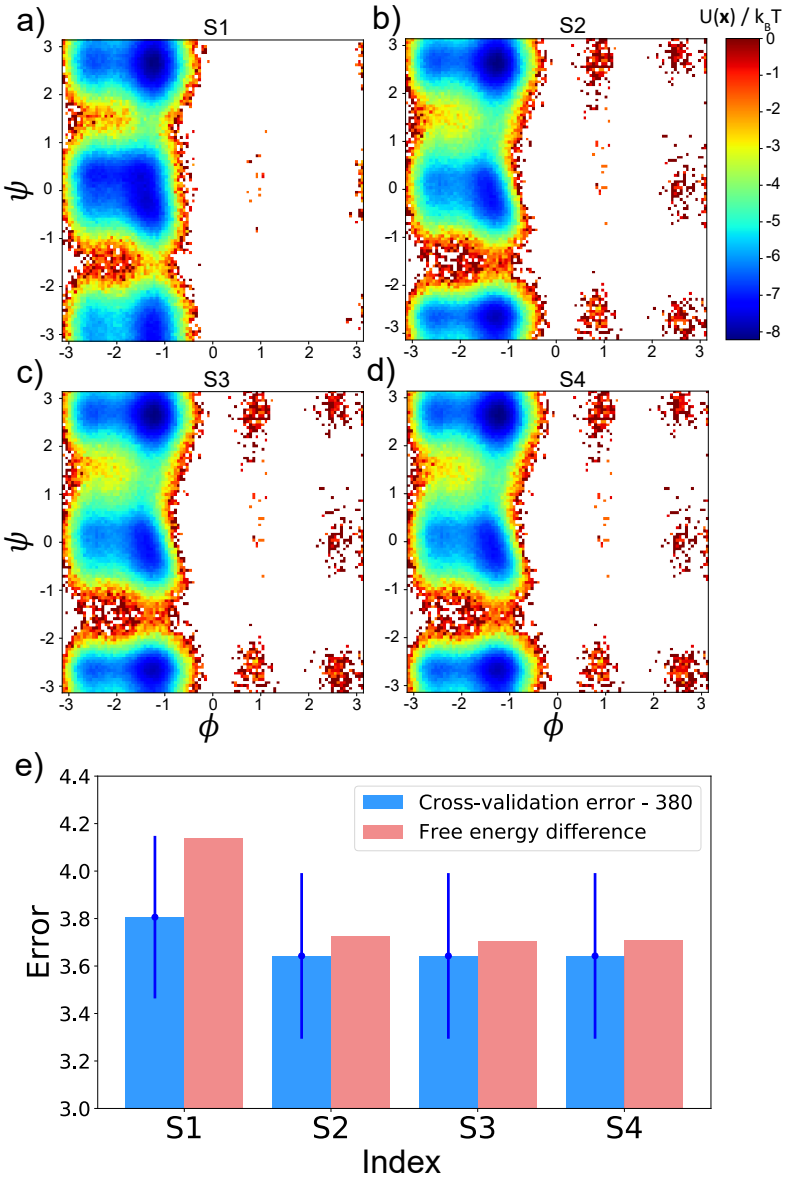


Figure S5: Comparison of the free energy profiles of the spline models of alanine dipeptide with different choices of hyper-parameters. (a)-(d) Free energy profiles with hyperparameters corresponding to the combination indicated as S1, S2, S3, S4 in Fig. 5. The choice of hyperparameters S4 correspond to the global optimum and is also reported in Fig. 6b. (e) Comparison between the cross validation error (in $[kcal/(mol{\cdot}\mathring{A})]^2$) and mean square free energy difference (in $[k_BT]^2$) for the five selected hyperparameters. The value of 380 is subtracted from the cross validation error to obtain values in the similar range as the free energy differences.

Energy decomposition for the CGnet model of alanine dipeptide.

As discussed in the main text, the use of a baseline energy to enforce physical constraints plays an important role in the CGnet model. Here we report the decomposition of the total CGnet energy into the contribution of the baseline (prior) energy and the energy of the neural network. Figs. S6a-c report the decomposition for each point sampled in the simulations performed with CGnet. Fig. S6d-f report the same quantity averaged over different bins in the space spanned by the dihedral angles. The figures show that the network energy captures the overall features of the free energy landscape for this molecule, while the prior energy seems to play an important role to enforce physical constraints mostly at the edges of the populated regions in the landscape. This is in agreement with the intuition that the prior energy term makes the system avoid high energy regions not visited in the training data.

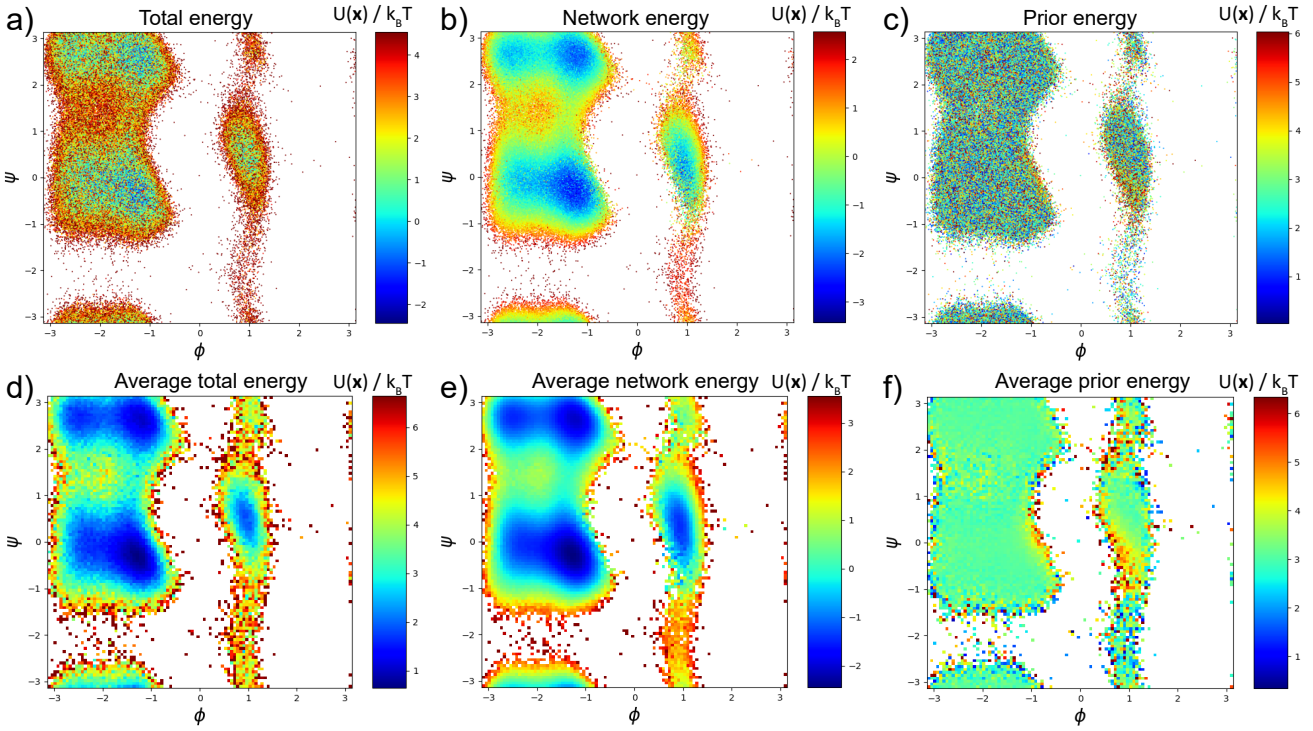


Figure S6: CGnet energy decomposition for the alanine dipeptide. In each simulated point, the total CGnet energy (a) is decomposed in the energy contribution from the dense net (b), and the baseline (or prior) energy (c). In each bin in the dihedral angles space, the average total total energy (d) is decomposed into the average dense net energy (e), and average prior energy (f).

Chignolin setup and simulation

The initial structure of Chignolin was generated starting from the cln025 peptide[3], with sequence TYR-TYR-ASP-PRO-GLU-THR-GLY-THR-TRP-TYR. The structure was solvated in a cubic box of 40 ÃĚ, containing 1881 water molecules and two Na^+ ions to neutralize the peptide's negative charge, as described in[4]. MD simulations were performed with ACEMD[5], using CHARMM22*[6] force field and TIP3P[7] water model at 350K temperature. A Langevin integrator was used with a damping constant of 0.1 ps^{-1}. Integration time step was set to 4 fs, with heavy hydrogen atoms (scaled up to four times the hydrogen mass) and holonomic constrains on all hydrogen-heavy atom bond terms[8]. Electrostatics were computed using Particle Mesh Ewald with a cutoff distance of 9 ÃĚ and grid spacing of 1 ÃĚ. Ten NVT simulations of 1 ns length were carried out, with a dielectric

constant of 80 and temperature of 350K to generate ten different starting conformations for the production runs. Production simulations consisted of 3744 independent simulations of 50 ns, for a total aggregate time of 187.2 μs. All the simulations were run using the GPUGRID[9] distributed computing platform. The first 1000 simulations were spawned from the 10 conformations obtained previously. The remaining 2744 simulations were spawned using the adaptive sampling[10] protocol implemented in HTMD[11]. In adaptive sampling, multiple rounds of simulations are performed, and each round the available trajectories are analyzed to select the initial coordinates for the next round of simulations. Each round was done every 10 to 20 simulations, respawning an equivalent amount of new simulations. Initial coordinates for the respawned simulations were selected proportionally to the inverse of the number of frames per macrostate as explained in[11]. The Markov State Model[12–16] constructed during the analysis was done using atom distances as projected metric, TICA[17,18] for dimensionality reduction method and k-Centers for clustering. Force data used for training CGnet was obtained from the MD simulation trajectories. ACEMD was used to read the Chignolin trajectories and compute forces for all atoms for each simulation frame, using the same parameters used for the MD simulations.

Markov State Model analysis of Chignolin all-atom simulations

MD simulation data of Chignolin from GPUGrid was featurized into all pairwise C_α distances excluding pairs of nearest neighbors residues (a total of 45 distances). Time-lagged independent component analysis (TICA)[17,18] was carried out with a lag $\tau = 25\,\text{ns}$. By using kinetic-map[19,20] and a kinetic variance cutoff of 95%, 4 TICs were retained for further analysis. The 4 TICs were clustered into 350 discrete states using the k-means algorithm. All MD data was mapped onto their discrete states and used for Markov state model (MSM) estimation. The implied-timescales, $t_i = -\frac{\tau}{\log|\lambda_i|}$, become constant as a function of lag-time (τ) within statistical uncertainty for lag-times above approximately 20 ns. Spectral analysis of a Markov state model estimated at a lagtime $\tau = 37.5\,\text{ns}$ reveal a spectral gap after the third implied-timescale suggesting 4 meta-stable states (Fig. S7). Plotting the populations of the meta-stable states as function of lag-time show that these are stable for $\tau > 10\,\text{ns}$, and that three of the four meta-stable states have significant probability mass $> 1\%$. These three most stable meta-stable states were used as reference states a, b and c, ordered alphabetically from most to least populated (shown in Fig. 7a). To account for the non-equilibrium nature of the multiple short molecular dynamics trajectories, we used the estimated MSM ($\tau = 37.5\,\text{ns}$) to reweighed data prior to calculating the reference free energy profiles. These analyses were carried out using the PyEMMA[21] and MDTraj[22] software packages.

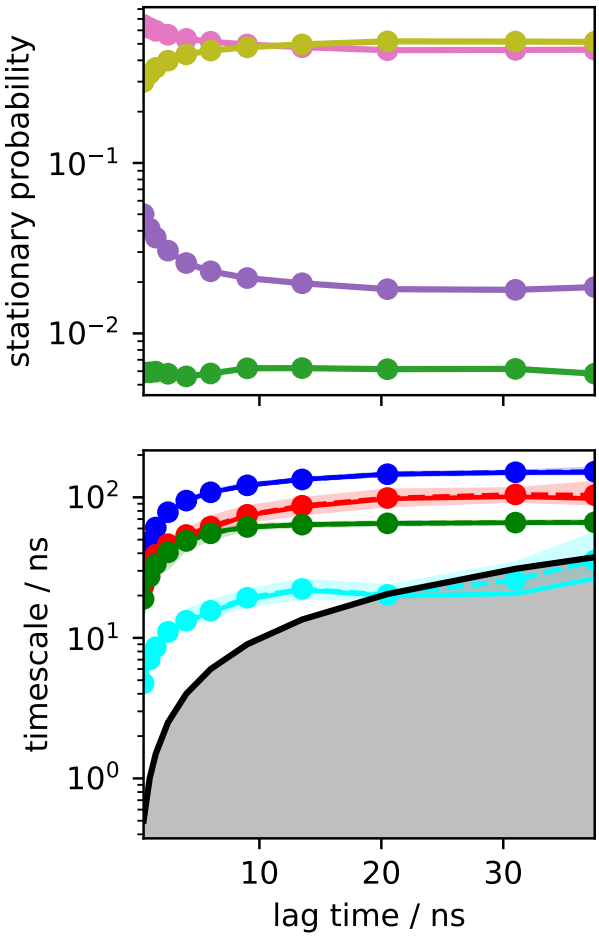


Figure S7: Validation of a convergence of the Chignolin all-atom Markov model, which is estimated at $\tau = 37.5\,\mathrm{ns}$. Top: Stationary probabilities of metastable states. Bottom: MSM implied time scales.

Hyper-parameter optimization for Chignolin CG models

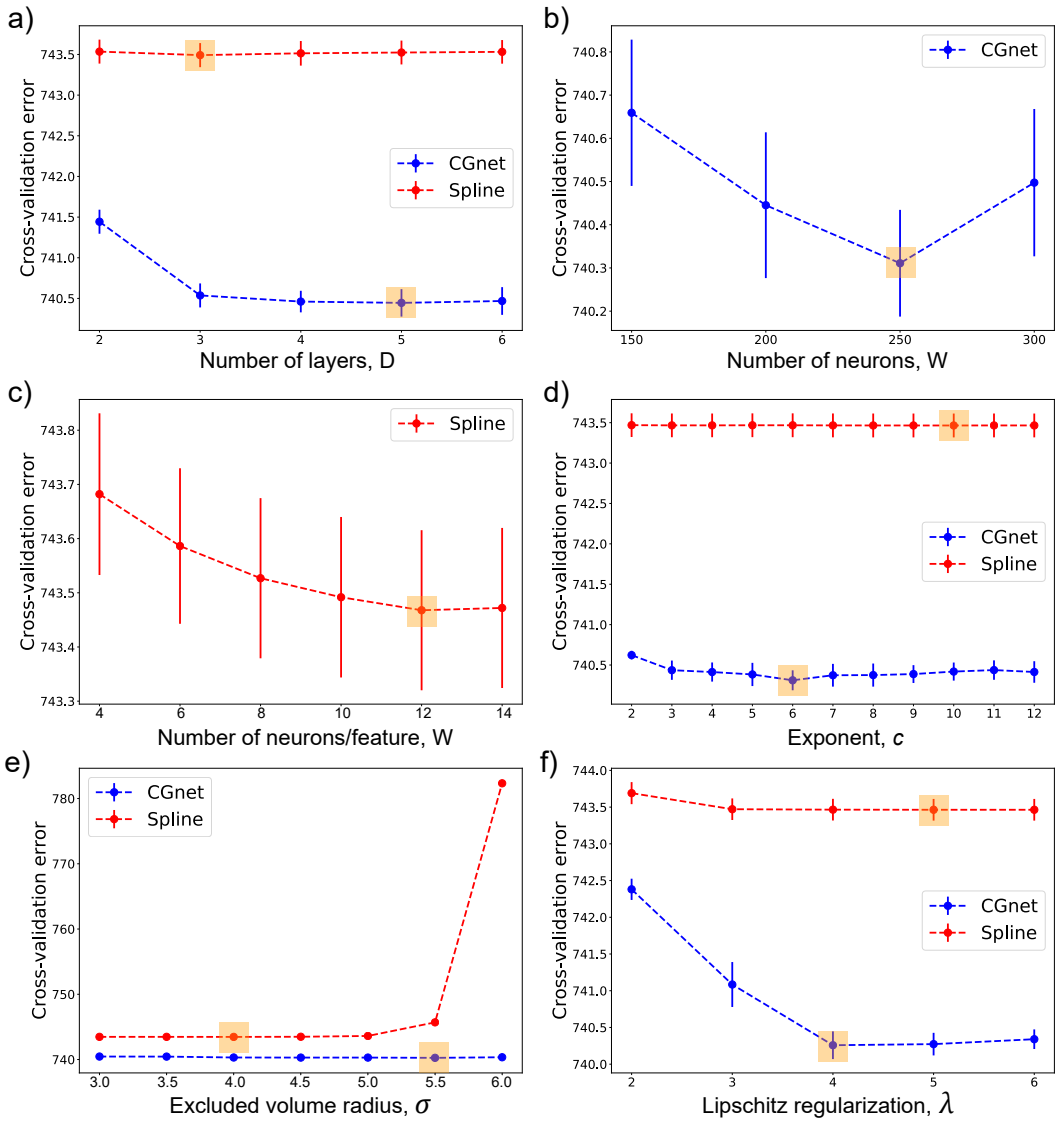


Figure S8: Five-stage cross-validation of the hyper-parameters for the CG models of Chignolin. (a) Selection of the number of layers, D. (b) and (c) Selection of the number of neurons per layer, W. (d) Selection of the exponent of the excluded volume term, c. (d) Selection of the effective excluded volume radius, σ. (f) Selection of of the Lipschitz regularization strength, λ. The optimal values are indicated by orange squares and are used to generate the results reported in Fig. 7.

References

(1) L. Boninsegna, F. Nüske, and C. Clementi. Sparse learning of stochastic dynamical equations. *J. Chem. Phys.*, 148(24):241723, 2018.

(2) D. P. Kingma and J. Ba. Adam: A method for stochastic optimization. *arXiv:1412.6980*, 2014.

(3) S. Honda, T. Akiba, Y. S. Kato, Y. Sawada, M. Sekijima, M. Ishimura, A. Ooishi, H. Watan-

abe, T. Odahara, and K. Harata. Crystal structure of a ten-amino acid protein. *J. Am. Chem. Soc.*, 130(46):15327–15331, 2008.

(4) K. Lindorff-Larsen, S. Piana, R. O. Dror, and D. E. Shaw. How fast-folding proteins fold. *Science*, 334(6055):517–20, 2011.

(5) M. J. Harvey, G. Giupponi, and G. De Fabritiis. ACEMD: Accelerating biomolecular dynamics in the microsecond time scale. *J. Chem. Theory Comput.*, 5(6):1632–1639, 2009.

(6) S. Piana, K. Lindorff-Larsen, and D. E. Shaw. How robust are protein folding simulations with respect to force field parameterization? *Biophys. J.*, 100(9):L47–L49, 2011.

(7) W. L. Jorgensen, J. Chandrasekhar, J. D. Madura, R. W. Impey, and M. L. Klein. Comparison of simple potential functions for simulating liquid water. *J. Chem. Phys.*, 79(2):926–935, 1983.

(8) K. A. Feenstra, B. Hess, and H. J. Berendsen. Improving efficiency of large time-scale molecular dynamics simulations of hydrogen-rich systems. *J. Comput. Chem.*, 20(8):786–798, 1999.

(9) I. Buch, M. J. Harvey, T. Giorgino, D. P. Anderson, and G. De Fabritiis. High-throughput all-atom molecular dynamics simulations using distributed computing. *J. Chem. Inf. Model.*, 50(3):397–403, 2010.

(10) S. Doerr and G. De Fabritiis. On-the-Fly Learning and Sampling of Ligand Binding by High-Throughput Molecular Simulations. *J. Chem. Theory Comput.*, 10(5):2064–2069, 2014.

(11) S. Doerr, M. J. Harvey, F. Noé, and G. De Fabritiis. HTMD: High-Throughput Molecular Dynamics for Molecular Discovery. *J. Chem. Theory Comput.*, 12(4):1845–1852, 2016.

(12) J.-H. Prinz, H. Wu, M. Sarich, B. G. Keller, M. Senne, M. Held, J. D. Chodera, C. Schütte, and F. Noé. Markov models of molecular kinetics: Generation and validation. *J. Chem. Phys.*, 134:174105, 2011.

(13) W. C. Swope, J. W. Pitera, and F. Suits. Describing protein folding kinetics by molecular dynamics simulations: 1. Theory. *J. Phys. Chem. B*, 108:6571–6581, 2004.

(14) J. D. Chodera, K. A. Dill, N. Singhal, V. S. Pande, W. C. Swope, and J. W. Pitera. Automatic discovery of metastable states for the construction of Markov models of macromolecular conformational dynamics. *J. Chem. Phys.*, 126:155101, 2007.

(15) F. Noé, I. Horenko, C. Schütte, and J. C. Smith. Hierarchical Analysis of Conformational Dynamics in Biomolecules: Transition Networks of Metastable States. *J. Chem. Phys.*, 126:155102, 2007.

(16) N. V. Buchete and G. Hummer. Coarse Master Equations for Peptide Folding Dynamics. *J. Phys. Chem. B*, 112:6057–6069, 2008.

(17) G. Perez-Hernandez, F. Paul, T. Giorgino, G. D Fabritiis, and F. Noé. Identification of slow molecular order parameters for markov model construction. *J. Chem. Phys.*, 139:015102, 2013.

(18) C. R. Schwantes and V. S. Pande. Improvements in markov state model construction reveal many non-native interactions in the folding of ntl9. *J. Chem. Theory Comput.*, 9:2000–2009, 2013.

(19) F. Noé and C. Clementi. Kinetic distance and kinetic maps from molecular dynamics simulation. *J. Chem. Theory Comput.*, 11:5002–5011, 2015.

(20) F. Noé, R. Banisch, and C. Clementi. Commute maps: separating slowly-mixing molecular configurations for kinetic modeling. *J. Chem. Theory Comput.*, 12:5620–5630, 2016.

(21) M. K. Scherer, B. Trendelkamp-Schroer, F. Paul, G. Perez-Hernandez, M. Hoffmann, N. Plattner, C. Wehmeyer, J.-H. Prinz, and F. Noé. PyEMMA 2: A software package for estimation, validation and analysis of Markov models. *J. Chem. Theory Comput.*, 11:5525–5542, 2015.

(22) R. T. McGibbon, K. A. Beauchamp, M. P. Harrigan, C. Klein, J. M. Swails, C. X. Hernández, C. R. Schwantes, L. P. Wang, T. J. Lane, and V. S. Pande. Mdtraj: A modern open library for the analysis of molecular dynamics trajectories. *Biophys J.*, 109:1528–1532, 2015.